A&A manuscript no.
(will be inserted by hand later)

Your thesaurus codes are:
02(11.19.3; 11.14.1; 11.01.2; 11.19.7; 09.08.1; 13.09.1)

ASTRONOMY
AND
ASTROPHYSICS
5.2.2008

Starbursts in barred spiral galaxies

III. Definition of a homogeneous sample of Starburst Nucleus Galaxies ⋆

T. Contini[1,2], **S. Considère**[3], **and E. Davoust**[1]

[1] Observatoire Midi-Pyrénées, UMR 5572, 14 Avenue E. Belin, F-31400 Toulouse, France
[2] School of Physics & Astronomy, Tel-Aviv University, 69978 Tel-Aviv, Israel
[3] Observatoire de Besançon, UPRES-A 6091, B.P. 1615, F-25010 Besançon Cedex, France

Received 30 September 1997; accepted 1 December 1997

Abstract. This paper presents optical long-slit spectroscopic observations of 105 barred Markarian IRAS galaxies. These observations are used to determine the spectral type (starburst or Seyfert) of emission-line regions in the nucleus and along the bar of the galaxies, in order to define a homogeneous sample of Starburst Nucleus Galaxies (SBNGs).

Our selection criteria (ultraviolet excess, far infrared emission and barred morphology) have been very efficient for selecting star-forming galaxies, since our sample of 221 emission-line regions includes 82% nuclear or extranuclear starbursts. The contamination by Seyferts is low (9%). The remaining galaxies (9%) are objects with ambiguous classification (HII or LINER).

The dust content and Hα luminosity increase towards the nuclei of the galaxies. No significant variation of the electron density is found between nuclear and bar HII regions. However, the mean Hα luminosity and electron density in the bar are higher than in typical disk HII regions.

We investigate different mechanisms for explaining the excess of nitrogen emission observed in our starburst nuclei. There is no evidence for the presence of a weak hidden active galactic nucleus in our starburst galaxies. The cause of this excess is probably a selective enrichment of nitrogen in the nuclei of the galaxies, following a succession of short and intense bursts of star formation.

Our sample of SBNGs, located at a mean redshift of ~ 0.015, has moderate Hα ($\sim 10^{41}$ erg s^{-1}) and far infrared ($\sim 10^{10}$ L$_\odot$) luminosities. The types are distributed equally among early- and late-type giant spirals with a slight preference for Sbc/Sc types because of their barred morphology. The majority (62%) of SBNGs are isolated with no sign of gravitational interaction. In terms of distance, luminosity and level of interaction, SBNGs are intermediate between HII galaxies and luminous infrared galaxies.

Key words: galaxies: starburst – galaxies: nuclei – galaxies: active – galaxies: statistics – HII regions – infrared: galaxies

1. Introduction

Our present knowledge of the properties of starburst galaxies, and of the physical conditions in nuclei and in extranuclear HII regions of spiral galaxies, rests on the analyses of a rather limited number of data sets. The selection criteria for the various samples necessarily introduce biases which influence the derived properties and which might explain why these studies sometimes reach conflicting results, for example on the role of the bar or of gravitational interactions in triggering starbursts. It is thus essential to multiply the observations of starburst galaxies, in order to make available the largest possible dataset for future analyses.

The goal of the present paper is to present a new sample of starburst galaxies which differs markedly in its selection from other samples. We wanted to avoid selecting small metal-poor galaxies (such as blue compact dwarfs) preferentially found in objective prism surveys, monsters (such as mergers or ultraluminous infrared galaxies) selected because of their unusual shape or luminosity, and

Send offprint requests to: T. Contini, contini@wise.tau.ac.il

⋆ Based on observations obtained at the 1.93 meter telescope of Observatoire de Haute-Provence operated by INSU (CNRS). Tables 1, 3, 4, 5 and 6 are only available in electronic form at the CDS via anonymous ftp to `cdsarc.u-strasbg.fr (130.79.128.5)` or via `http://cdsweb.u-strasbg.fr/Abstract.html`

active galaxies (such as Seyferts), which are probably related to starbursts, but should be considered separately. We thus devised selection criteria that would enable us to catch in our nets galaxies preferably resembling rather "normal" giant spiral galaxies. We believe that we have been fairly successful, and this new sample has been subjected to an extensive multifrequency analysis (Contini 1996), the results of which have been or will be reported separately (see Sect. 7).

2. The original sample

2.1. Selection criteria

We defined three criteria for selecting a sample of galaxies likely to contain the highest number of starburst galaxies. The selected galaxies must possess:

1. an excess of blue and ultraviolet (UV) emission; this would indicate the presence of a large number of young and hot stars.
2. A strong far-infrared (FIR) emission; interstellar dust heated by the UV radiation field from the young and hot stars is likely to give rise to such an emission.
3. A barred morphology; a bar is expected to enhance the gas flow toward the center of galaxies and may provide a mechanism for triggering nuclear starbursts.

The Markarian survey contains 1500 objects selected for their excess of blue and UV emission among which about 1100 are galaxies. The catalog of Markarian galaxies is the largest sample of active galaxies known so far. The excess of blue luminosity and UV emission is the signature of either a high star formation rate or the presence of an Active Galactic Nucleus (AGN) in the central region of the galaxies. We extracted our sample from the extensive compilation of Markarian galaxies by Mazzarella & Balzano (1986) which lists valuable data, such as morphology, magnitude, radial velocity, radio (6, 11 and 21 cm continuum) and infrared (60 μm) flux of the galaxies.

The very successful IRAS mission, which covered about 98% of the sky in four bands centered at 12, 25, 60 and 100 μm has led to valuable information on the origin of the FIR radiation and its relation to the dust content of star forming regions. Interstellar dust is heated by absorption of a large fraction of UV radiation and this energy is reradiated in the FIR range. In most IRAS galaxies, the heating of interstellar dust is due to a high star formation rate and/or an AGN which provides a sufficiently strong ionizing flux to produce the observed FIR radiation. We thus selected those galaxies of the Markarian catalog which were detected by the IRAS satellite, and listed in two catalogs of IRAS sources, namely the Point Source Catalog (PSC) which contains all the bright point sources and the Faint Source Catalog (FSC) which contains fainter extended sources.

With the first two criteria (UV- and FIR-bright), we expected to select a sample of galaxies with a high proportion of starburst galaxies. Our last criterion was to select galaxies with a barred morphology, because of their peculiar dynamics. The bar is thought to enhance the flow of molecular gas toward the center of spiral galaxies where a high concentration of this gas will trigger nuclear starbursts. To select galaxies with bars, we used the morphological classifications provided by Mazzarella & Balzano (1986) and LEDA (Lyon-Meudon Extragalactic Database).

Finally, the combination of two activity criteria (Markarian + IRAS) and the presence of a bar defined a sample of 144 barred Markarian IRAS galaxies.

This sample differs from others used for studying the starburst phenomenon in galaxies. Indeed, many works in this field are based on samples of small irregular or blue compact dwarf galaxies like "HII galaxies" (e.g. Terlevich et al. 1991), or samples of highly luminous infrared galaxies (e.g. Veilleux et al. 1995), or even very heterogeneous samples of galaxies of mixed types. Our sample is of course not free from selection effects; the first selection criterion excludes galaxies with little or no UV excess, the second one discriminates against weaker starbursts, with less dust and molecular gas, the third one favors late-type galaxies, and the Markarian catalogue does not contain nearby star-forming galaxies (such as M82 or NGC 253).

2.2. Global properties of the sample

The global properties of the original sample are listed in Table 1. The first column gives the number of the galaxy in the Markarian catalog. Columns 2 and 3 indicate the equatorial coordinates (equinox 1950). Cross identifications with other catalogs are given in column 4. The morphological properties of the galaxies, based on the classification system of de Vaucouleurs et al. (1991, RC3), are given in columns 5 to 8. Column 6 indicates if the galaxy has ring structures and column 7 if it belongs to a multiple system. The inclination and heliocentric radial velocity are given in columns 9 and 10. The apparent blue magnitude, corrected for both Galactic and internal extinction with the method of de Vaucouleurs et al. (1991, RC3), and the absolute blue magnitude are reported in columns 11 and 12. All the above general properties come from LEDA.

The IRAS data, reported in columns 13 to 20 of Table 1, come from the *Faint Source Survey* (Bicay et al. 1995). These data are more accurate than those from the PSC or the FSC, and represent in fact the latest version of the IRAS catalog. The flux densities (in Jy) at 12, 25, 60 and 100 μm are reported in columns 14, 16, 18 and 20 respectively. A quality code is assigned to each flux density in order to evaluate the reliability of the measurements. The code value is equal to 3 if the measurement is of high quality, to 2 if the quality is moderate

and to 1 if it corresponds to an upper limit (90% confidence level). No measurements of the flux density at 100 μm are reported with a quality code greater than or equal to 3, because of the strong contamination by interstellar cirrus at this wavelength. Table 1 is given in electronic form only.

These data will be used in Sect. 6 to derive the general properties of the SBNGs.

Table 1. Global properties of the sample of barred Markarian galaxies

Table 2. Characteristics of CCD cameras and spectrophotometric standard stars used for each observing run

Observing run	CCD camera			standard
	Type	Size (pixels)	pixel size	star
April 1991	RCA 3	323 × 512	30 μm	GD140
September 1991	RCA 1	323 × 512	30 μm	G191B2B
January 1992	THX1	405 × 581	23 μm	
March 1992	TK512	512 × 512	27 μm	BD2626
Feb.-March 1993	TK512	512 × 512	27 μm	GD140
December 1993	TK512	512 × 512	27 μm	Hiltner 600
January 1994	TK512	512 × 512	27 μm	Hiltner 600

Table 3. Log of spectroscopic observations

3. Observations

The spectroscopic observations were obtained at the 1.93 meter telescope of Observatoire de Haute-Provence between April 1991 and January 1994. The data were acquired with the CARELEC spectrograph (Lemaître et al. 1990) and several types of CCD cameras (see Table 2). The spectral resolution was 260 Å/mm, which provides a spectral coverage of $\sim$ 3800 − 7400 Å with a resolution $\Delta\lambda \sim 15$ Å. The spectra were acquired under good photometric conditions with a typical seeing between 2 and 3″.

During those nights, we also observed various spectrophotometric standard stars (see Table 2) taken from the list given by Massey et al. (1988), except for BD 2626 (Oke & Gunn 1983), in order to flux calibrate the galaxy spectra. He comparison line spectra were obtained immediately before and after the galaxy integration in order to calibrate accurately the wavelength scale. The slit was usually aligned along the bar of the galaxy. For galaxies with multiple nuclei or for pairs of galaxies, we oriented the slit in order to cover the brightest knots.

The observation log is given in Table 3, which gives for each galaxy (column 1) the date of observation (column 2), the exposure time (column 3), the spectral range (column 4), the width and position angle of the slit (columns 5 and 6). Table 3 is given in electronic form only. During the allocated telescope time, we were able to observe 105 of the 144 galaxies of the sample. The remainder of the paper is based on the data collected for these 105 galaxies.

4. Data reduction

The spectroscopic data were reduced with the MIDAS package LONG. The spectra were flux calibrated and corrected for foreground reddening using the method described by Contini, Davoust & Considère (1995, hereafter paper I).

In order to extract individual spectra of all (nuclear and extranuclear) emission-line regions for each galaxy spectrum, we plotted the spatial distribution of the Hα emission line along the slit. We then identified distinct regions of emission and measured their dimension and position along the slit by fitting multi-Gaussian profiles to the Hα spatial distribution.

We extracted one-dimensional elementary spectra by adding the columns (spatial dimension) corresponding to the dimension of each emission-line region estimated above. One can note at this stage that 42 galaxies do not have any extra-nuclear emission-line region along the slit (i.e. along the bar). The elementary spectra were cleaned of radiation events ("cosmic rays") before further analysis.

For measuring all the line parameters (fluxes, FWHM and equivalent widths), and for determining the internal reddening ($c_{\mathrm{H}\beta}$), we again followed the method described in paper I. For the latter determination, we adopted Case B of Balmer decrement ($I(\mathrm{H}\alpha)/I(\mathrm{H}\beta) = 2.85$) for classical H II regions, and Case A ($I(\mathrm{H}\alpha)/I(\mathrm{H}\beta) = 3.10$) for AGNs.

We also estimated the continuum flux density, f_λ, of the individual regions in three spectral bands labeled B (λ_c = 4200 Å and $\Delta\lambda$ = 300 Å), V (λ_c = 5400 Å and $\Delta\lambda$ = 300 Å) and R (λ_c = 6800 Å and $\Delta\lambda$ = 200 Å) very close to Johnson's photometric system. In order to obtain the continuum values in a consistent and objective manner, we measured the spectra with an automated algorithm. We chose the wavelength range of the spectral bands in such a way as to exclude the regions containing emission lines.

The measured emission lines are given in Table 4. The galaxy Markarian number is given in column 1. The label and code for the position of the emission-line regions (1 = nuclear, 0 = extranuclear) are given in columns 2 and 3. The distance of the extranuclear regions from the nucleus, and the diameter of all regions, expressed in arcsec, are given in columns 4 and 5. The observed fluxes $F(\lambda)$ and equivalent widths of Hβ, Hα (both corrected for Balmer absorption), [O III]λ4959, [O III]λ5007, [N II]λ6548, [N II]λ6583, [S II]λ6716 and [S II]λ6731 are listed in columns 6 to 21.

The continuum measurements are listed in Table 5. The galaxy Markarian number is given in column 1. The

magnitudes integrated along the slit ($m_{\rm B}$, $m_{\rm V}$ and $m_{\rm R}$) are given in columns 3, 4 and 5, where $m_\lambda = -2.5\log(f_\lambda) - 5\log(\lambda) - 2.41$, with f_λ in units of erg s^{-1} cm^{-2} Å^{-1} and λ in Å (Mazzarella & Boroson 1993). We further used the continuum magnitudes to define two color indices: $B-V = m_{\rm B} - m_{\rm V}$ and $V-R = m_{\rm V} - m_{\rm R}$ which are reported in column 6 and 7. Tables 4 and 5 are given in electronic form only.

Table 4. Measured spectrophotometric data. Observed intensities and equivalent widths of emission lines

Table 5. Measured spectrophotometric data. Magnitudes and color indices of the spectral continuum

5. Results

The characteristics of the emission-line regions and the derived spectrophotometric parameters are given in Table 6. The galaxy (Mrk) number is given in column 1. The label and code for the position of the emission-line regions (1 = nuclear, 0 = extranuclear) are repeated in columns 2 and 3. The distance of the galaxy, estimated using a Hubble constant of 75 kms^{-1}Mpc^{-1}, is given in column 4. The distance of the extranuclear regions from the nucleus, and the diameter of all regions, expressed in kpc, are given in columns 5 and 6. The reddening coefficient $c_{{\rm H}\beta}$ is given in column 7. The electronic density (n_e) is given in column 8. The line-intensity ratios, [N II]λ6583/Hα, [S II]$\lambda\lambda$6716,6731/Hα and [O III]λ5007/Hβ, used for the spectral classification and corrected both for internal reddening and for Balmer absorption, are reported in columns 9, 10 and 11, followed by the results of the spectral classification in column 12. The Hα flux [I(Hα) in 10^{-14} erg s^{-1} cm^{-2}] is given in column 13 and the Hα luminosity [L(Hα) in erg s^{-1}] in column 14. In the subsequent analysis we only take into account the Hα luminosities corrected for reddening, that is, those of galaxies for which we derived the reddening parameter $c_{{\rm H}\beta}$ (see Sect. 5.3). For the others, we give lower limits on the Hα flux and luminosity in Table 6, which is given in electronic form only.

Table 6. Derived spectrophotometric parameters

5.1. Spectral Classification

We used diagnostic diagrams (Baldwin, Phillips & Terlevich 1981, Veilleux & Osterbrock 1987) for identifying the various ionization mechanisms responsible for the emission-line regions of our galaxies. In these diagrams, one can distinguish regions photoionized by hot and young stars (i.e. HII regions) from those photoionized by a harder radiation field, such as that of an AGN or a LINER, using several ratios between low-ionization and Balmer emission lines.

At this stage, it is necessary to clarify the definition of the different types of starburst galaxies which will be mentioned in this paper. One can first separate HII galaxies and starburst galaxies by the properties of the host galaxy. HII galaxies are mainly metal-poor dwarf irregular or blue compact galaxies with low dust content (e.g. French 1980, Keel 1983 and Terlevich et al. 1991). They contain many giant HII regions with high-excitation spectra, with properties very close to those of extragalactic giant HII regions distributed in the disk of nearby spiral galaxies (e.g. McCall, Rybski & Shields 1985). HII nucleus galaxies (Stauffer 1982, Keel 1983, Kennicutt, Keel & Blaha 1989, Ho, Filippenko & Sargent 1997a) and Starburst Nucleus Galaxies (SBNGs; Balzano 1983, Coziol et al. 1994) are defined as galaxies with HII regions in their nuclei. They are more massive and chemically evolved spiral galaxies, with a large population of old and evolved stars and a huge quantity of dust (Coziol 1996). The low-excitation spectra of SBNGs reflect the higher metallicity observed in spiral galaxies, and especially in their nucleus, when compared to irregular or compact HII galaxies. A last distinction is made between HII nuclei and SBNGs on the basis of their nuclear Hα luminosity, HII nuclei being fainter (L(Hα) $\lesssim 10^{40}$ erg s^{-1}) than SBNGs. In terms of star formation, HII nuclei represent the low-luminosity end of SBNGs (Coziol 1996).

The results of our spectrophotometric analysis are displayed in Fig. 1 which shows the location of the emission-line regions in two diagnostic diagrams of Veilleux & Osterbrock (1987). In each diagram, the continuous curve, empirically derived by Veilleux & Osterbrock (1987), separates starburst nuclei and HII regions where the gas is assumed to be ionized by young stars, from AGNs where the main ionizing source is thought to be an accretion disk around a black hole (e.g. Rees 1984) which produces a power law spectrum. We make a further distinction among AGNs between objects of high ([O III]/H$\beta > 3$) and low ([O III]/H$\beta \leq 3$) excitation (horizontal line, Shuder & Osterbrock 1981). The first group represents the classical Seyfert 2 galaxies while the LINERs fall in the second group. We did not use the original criteria for defining a LINER (Heckman 1980) because measurements of [O I]λ6300 and [O II]λ3727 were often not available. For the same reason, we did not make

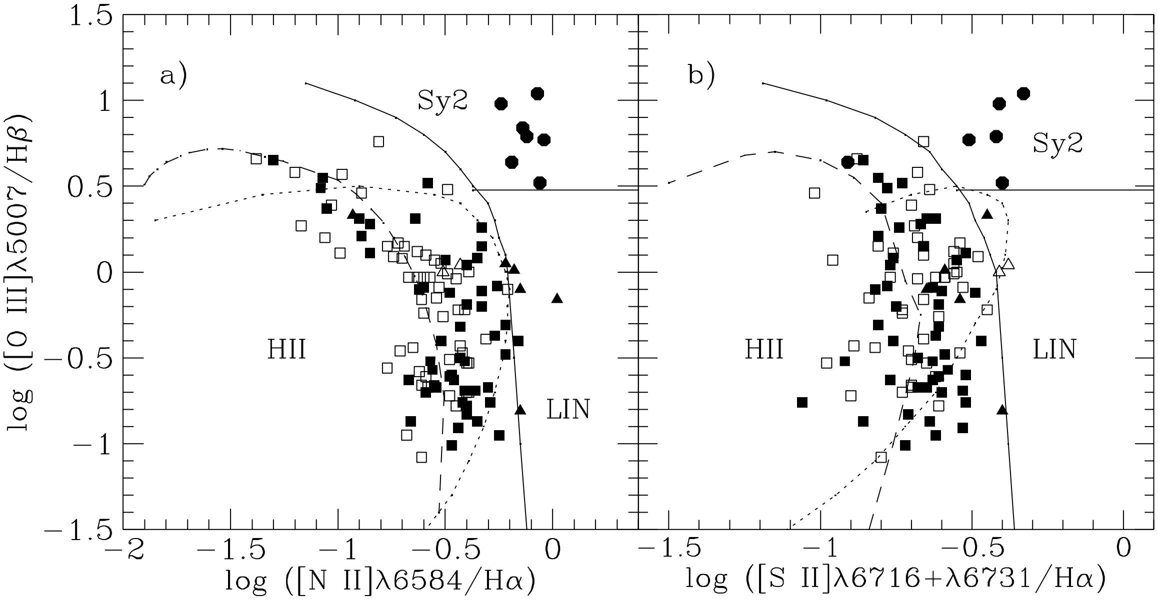

Fig. 1. Diagnostic diagrams, adapted from Veilleux & Osterbrock (1987), showing *a*) log([O III]λ5007/Hβ) vs. log([N II]λ6583/Hα) and *b*) log([O III]λ5007/Hβ) vs. log([S II]λλ6716,6731/Hα). The symbols are : *filled squares* = starburst nuclei, *open squares* = extranuclear HII regions, *filled circles* = Seyfert 2 nuclei and *triangle* = objects with an ambiguous classification (HII or LINER, see text). In each diagram two curves (*solid lines*) separate the emission-line regions in three groups: starburst galaxies or HII regions (lower left), Seyfert 2 galaxies (upper right) and LINERs (lower right). The *dashed curve* denotes the theoretical models of disk HII regions of McCall, Rybski & Shields (1985). Also shown is the photoionization model of Shields & Kennicutt (1995) (*dotted curve*)

use of the [O I]λ6300/Hα ratio to distinguish between the different sources of ionization.

Table 7. Spectral classification

Spectral Type[a]	Emission line region		**Total**
	Nuclear	Extranuclear	
HII	70 (67%)	81 (69%)	151 (68%)
SBNG	65 (62%)	...	...
HIIG	5 (5%)	...	...
AGN	20 (19%)	...	20 (9%)
Sey 1	12 (11%)	...	...
Sey 2	8 (8%)	...	...
HII, LINER?	11 (10%)	8 (7%)	19 (9%)
Uncertain	4 (4%)	27 (24%)	31 (14%)
Total	105 (100%)	116 (100%)	221 (100%)

[a] SBNG = Starburst Nucleus Galaxy; HIIG = HII galaxy; HII, LINER? = ambiguous classification between HII and LINER (see text for details); Uncertain = classification based on only one emission line ratio ([N II]/Hα or [S II]/Hα)

One should note that the classification process is not always unambiguous, for at least two reasons. First, the two conditions involving the low-ionization lines ([N II] and [S II]) do not always hold simultaneously. This reflects the empirical nature of the diagnostic diagrams as well as the possibility that one line ratio is enhanced or depressed with respect to the other one as a result of, for instance, selective abundance variations (see Sect. 5.5.2). Second, large measurement uncertainties may be associated with any given line intensity ratio. Thus, one should evaluate each object individually, taking all of these factors into consideration, before a classification can be assigned to it. When more than one classification is consistent with the data, both are given, with the more likely one listed first (column 12 of Table 6). An ambiguous spectral classification (between HII and LINER) arises for 11 nuclear (Mrk 90, 271, 332, 353, 593, 617, 874, 1180, 1200, 1291 and 1485) and 8 extranuclear (Mrk 712-3, 814-1, 814-4, 1086-3, 1302-1, 1363-1, 1363-3 and 1433-3) regions.

The result of the spectral classification is summarized in Table 7. We found that 70 nuclear regions (67% of the sample) have spectra characteristic of photoionization by hot stars, i.e. are classified as starburst nuclei (62%) or HII galaxy (5%). Four galaxies (Mrk 21, 271, 446 and 1452) were classified as SBNGs using only one emission-line ratio ([N II]/Hα or [S II]/Hα), their classification is thus rather uncertain. AGN emission lines were observed in 20 nuclei (19%) including 12 Seyfert 1 galaxies (11%) and 8 Seyfert 2 galaxies (8%). Among the 116 extranuclear regions, 81 (69%) are HII regions. Here, the classification

is uncertain for 27 regions (24%) and ambiguous between HII and LINER for 8 regions (7%) for the same reason as explained above.

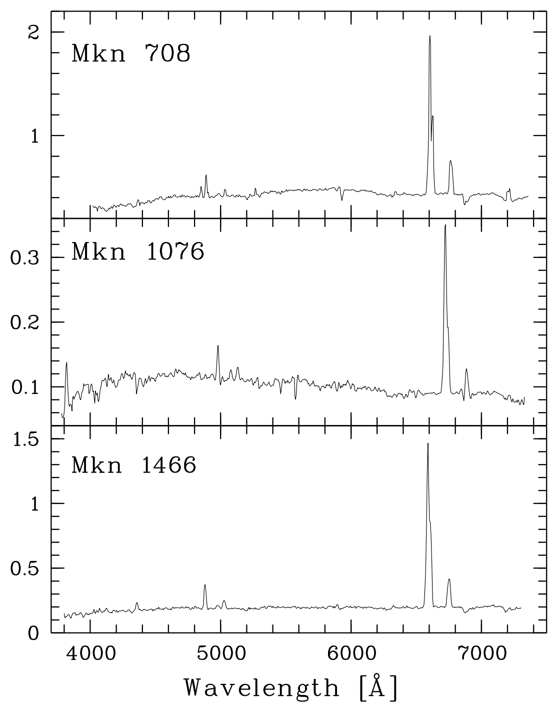

Fig. 2. Optical spectra of starburst nuclei. Intensities are in 10^{-14} erg s^{-1} cm^{-2} Å^{-1}

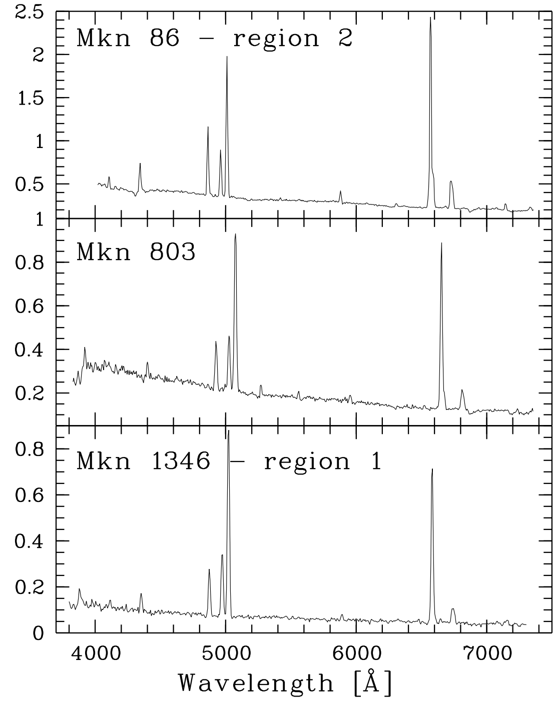

Fig. 3. Optical spectra of HII galaxies showing strong emission lines and a high excitation ([O III]/H$\beta > 3$) compared to starburst nuclei. Intensities are in 10^{-14} erg s^{-1} cm^{-2} Å^{-1}

Representative spectra of each spectral class are shown in Fig. 2 (starburst nuclei), Fig. 3 (HII galaxies), Fig. 4 (Seyfert 1 nuclei), Fig. 5 (Seyfert 2 nuclei), and Fig. 6 (objects with an ambiguous classification).

5.2. Colors

We corrected for reddening the spectral continuum colors $(B-V)$ and $(V-R)$ of the individual regions using the reddening coefficient $c_{\mathrm{H}\beta}$ and assuming that the interstellar extinction applies in the same way for the stellar population and the ionized gas in emission-lines regions.

A color-color diagram with the dereddened color indices $(B-V)_0$ and $(V-R)_0$ is shown in Fig. 7. The extranuclear HII regions and starburst nuclei are well mixed in this diagram, indicating identical stellar populations born during the same star formation episode. We first compare the colors of these starburst regions to the total color indices of "normal" galaxies. It comes as no surprise that they are much bluer than quiescent galaxies whose position is indicated by the dotted rectangle in Fig. 7; the vast majority of our starburst regions are located outside this rectangle traced by about 500 normal galaxies (Buta & Williams 1995). We then use the predictions of stellar population synthesis models of

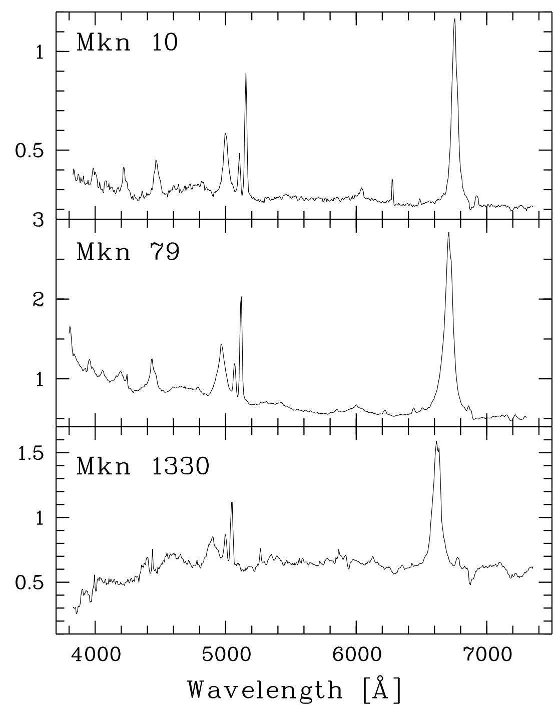

Fig. 4. Optical spectra of Seyfert 1 nuclei. The broad Balmer emission lines (Hα, Hβ, etc), compared to the narrower forbidden lines (e.g. [O III]), allow a clear and rapid classification of these AGNs. Intensities are in 10^{-14} erg s^{-1} cm^{-2} Å^{-1}

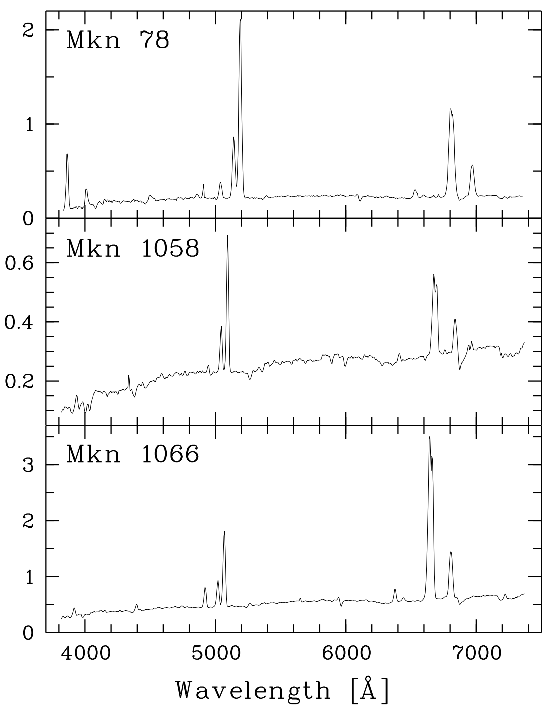

Fig. 5. Optical spectra of Seyfert 2 nuclei. In these AGNs, the Balmer lines have the same width as the forbidden lines and the excitation is high ([O III]/H$\beta > 3$). Intensities are in 10^{-14} erg s^{-1} cm^{-2} Å^{-1}

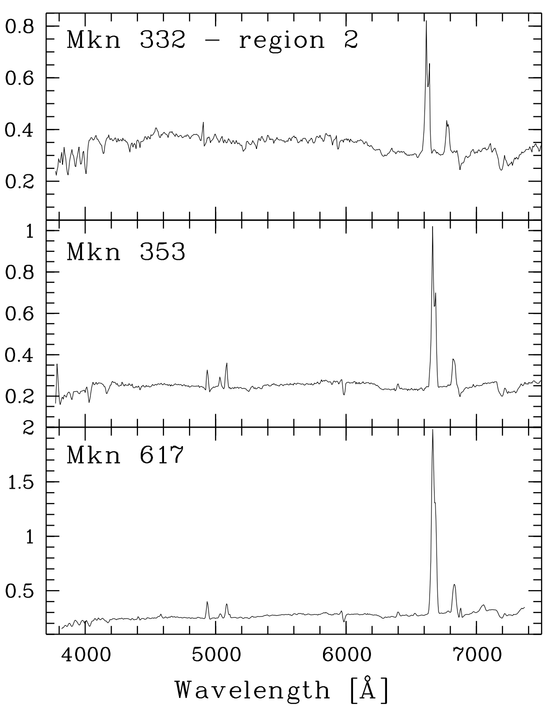

Fig. 6. Examples of objects with an ambiguous classification between HII and LINER. Intensities are in 10^{-14} erg s^{-1} cm^{-2} Å^{-1}

Leitherer & Heckman (1995) to estimate the age of the stellar population which dominates the spectral continuum of these starburst regions. It appears clearly that the colors observed in the star-forming regions are well fitted by a very young stellar population with an age lower than 50 Myr.

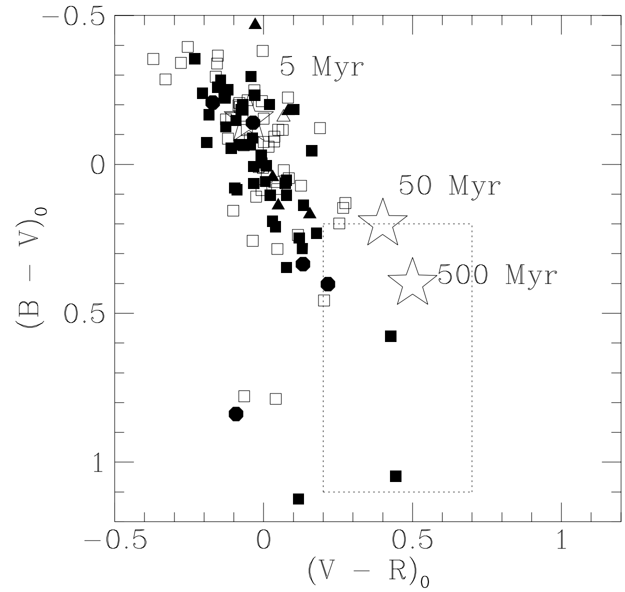

Fig. 7. Dereddened color-color diagram. The symbols have the same meaning as in Fig. 1. The dotted rectangle indicates the position of a sample of 500 normal galaxies (Buta & Williams 1995). The predictions of stellar population synthesis models of Leitherer & Heckman (1995) are indicated by the big stars for 5, 50 and 500 Myr

5.3. Reddening

The distribution of reddening ($c_{\mathrm{H}\beta}$) in the different emission-line regions is given in column 7 of Table 6 and shown in Fig. 8a. The amount of reddening is larger in starburst nuclei ($c_{\mathrm{H}\beta} = 0.81 \pm 0.38$) than in extranuclear HII regions (0.61 ± 0.28). When compared to other samples of starburst galaxies, the mean extinction coefficient derived in our sample is slightly larger than in nearby HII nuclei ($c_{\mathrm{H}\beta} \sim 0.42$, Ho, Filippenko & Sargent 1997a) and disk HII regions ($c_{\mathrm{H}\beta} \sim 0.29$, Kennicutt, Keel & Blaha 1989) but low compared to a sample of luminous infrared starburst galaxies ($c_{\mathrm{H}\beta} \sim 0.99$, Veilleux et al. 1995).

The amount of reddening has not been estimated for 13 nuclear and 35 extranuclear emission-line regions because of the weakness or absence of Hβ emission in their spectra. In all these objects we detect a relatively strong Hα emission; they are thus probably highly obscured. Note that in a few objects (nucleus of Mrk 52, extranuclear regions of Mrk 489 and 712), the observed Balmer decrement is

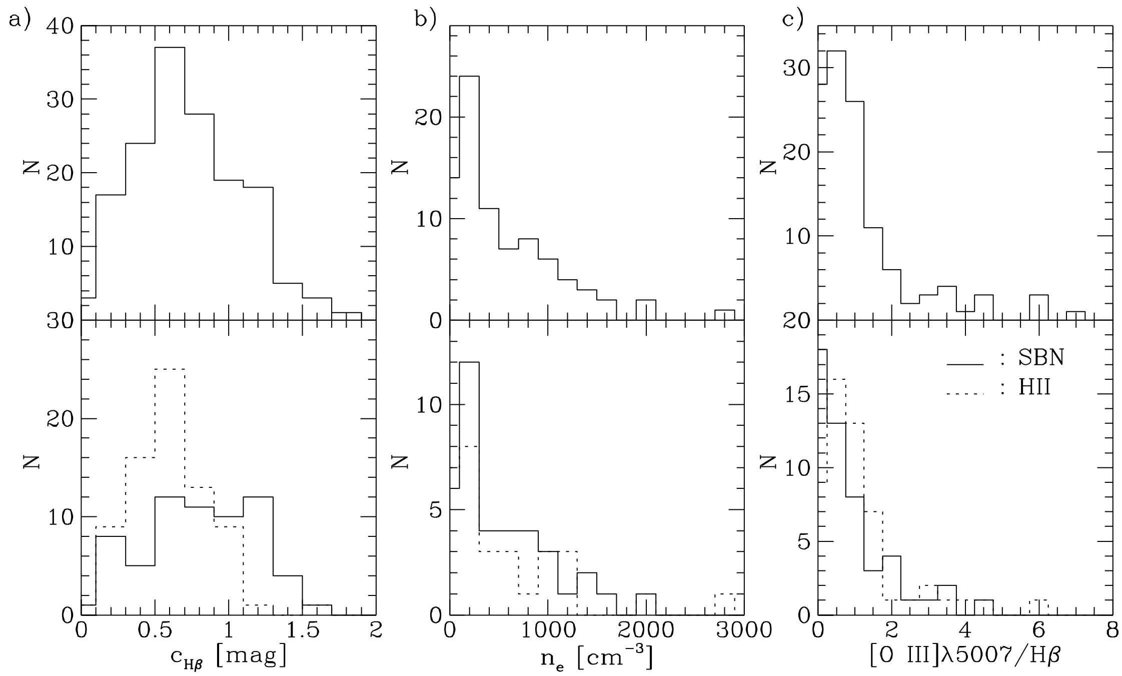

Fig. 8. Distribution of a) the extinction coefficient $c_{\mathrm{H}\beta}$, b) the electron density n_{e} and c) the excitation parameter [O III]λ5007/Hβ for all the emission-lines regions (*top*), for the starburst nuclei (SBN) and the extranuclear HII regions (HII) (*bottom*)

significantly less than the theoretical value; we assigned an internal extinction of zero to these objects.

5.4. Electron density

We derived the electron density (n_e) from the reddening-corrected [S II]λ6716/[S II]λ6731 line ratio using the analytical relation given by Osterbrock (1989). A 20% uncertainty in the [S II]λ6716/[S II]λ6731 flux ratio corresponds to an uncertainty of about 100 cm^{-3} in the determination of n_e.

Figure 8b shows the distribution of the electron densities for the different emission-line regions. The mean value of the electron density is nearly the same for nuclear starbursts (560±240 cm^{-3}) and extranuclear HII regions (770±500 cm^{-3}). These mean values are higher than those derived for nearby HII nuclei (180±200 cm^{-3}, Ho, Filippenko & Sargent 1997a), disk HII regions ($\sim$ 140 cm^{-3}, Kennicutt, Keel & Blaha 1989) and luminous infrared starburst galaxies ($\sim$ 280 cm^{-3}, Veilleux et al. 1995).

5.5. Line-intensity ratios

5.5.1. [O III]/Hβ as an excitation parameter

Two types of starburst galaxies can be distinguished based on their level of excitation: SBNGs show low-excitation spectra ([O III]/Hβ $<$ 3, see Fig. 2) whereas HII galaxies show high-excitation spectra ([O III]/Hβ $\geq$ 3, see Fig. 3).

A quick inspection of Fig. 1 indicates that the upper left region of the diagnostic diagrams contains only a few data points, reflecting the fact that essentially all the emission-line regions classified as starbursts have a relatively low excitation level ([O III]/Hβ $\leq$ 3). This is to be contrasted with Figs. 1–3 of Veilleux & Osterbrock (1987) where this region of the diagrams is populated with extranuclear HII regions and the low-metallicity HII galaxies from the sample of French (1980).

The distribution of the excitation parameter is shown in Fig. 8c. Our sample is obviously deficient in HII galaxies, since only five starburst galaxies (Mrk 86, 412, 803, 860 and 1346) have an excitation parameter [O III]/Hβ $\geq$ 3. The properties of these galaxies (listed in Table 1) indicate that they are mainly small, irregular and low-mass galaxies with a low dust content, confirming the general trend of this class of starburst galaxies (Coziol 1996). Our sample thus contains a vast majority of starburst nuclei located in more massive and chemically evolved galaxies than HII galaxies because of their higher frequency of past bursts of star formation (Coziol 1996). Note however that SBNGs are still in the process of formation because of their lower metal content compared to "normal" spiral galaxies (Coziol et al. 1997a). Figure 8c also shows that the mean excitation parameter is slightly higher in extranuclear HII regions ([O III]/Hβ $\sim$ 0.72) than in starburst nuclei ([O III]/Hβ $\sim$ 0.50), reflecting the negative abundance gradient from the nucleus to the outer parts of spiral galaxies.

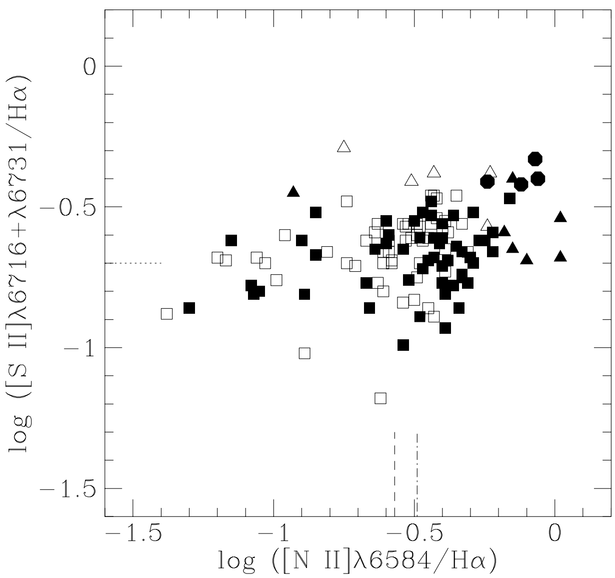

Fig. 9. Diagram of [S ii]/Hα as a function of [N ii]/Hα. The symbols have the same meaning as in Fig. 1. The mean value of [N ii]/Hα is higher in starburst nuclei (*dotted-dashed line*) than in extranuclear Hii region (*dashed line*) whereas the mean values of [S ii]/Hα are identical (*dotted line*)

Three Wolf-Rayet galaxies are present in our sample. The optical spectrum of this subset of starburst galaxies shows broad emission lines from Wolf-Rayet stars around $\sim$ 4700 Å, the brightest line being He iiλ4686. While Mrk 52 and Mrk 710 were already known Wolf-Rayet galaxies and included in the catalog of Conti (1991), a new one, Mrk 712, was discovered in the sample (paper I).

5.5.2. Excess of [N ii]/Hα in starburst nuclei

Excess emission of [N ii] has been reported in samples of emission line galaxies, such as SBNGs (Coziol et al. 1997b) or Hii nuclei (Ho, Filippenko & Sargent 1997a) with a mean ratio of log([N ii]/Hα) 0.2 to 0.3 dex higher than the mean ratio observed in disk Hii regions or predicted by normal Hii regions models (e.g. McCall, Rybski & Shields 1985).

In the diagnostic diagram of Fig. 1a, one can see that, for a given excitation parameter, our nuclear starbursts tend to have stronger [N ii]λ6583 emission than extranuclear Hii regions, but the difference is rather small ($<$ 0.1 dex) compared to other samples of starburst nuclei cited above.

This excess of nitrogen emission was first noted by Stauffer (1982) in the nuclei of "normal" galaxies and confirmed later in a sample of "Hii region-like" nuclei by Kennicutt, Keel & Blaha (1989) who proposed the presence of a hidden weak AGN to account for this excess of low-ionisation emission line. AGNs indeed produce a harder ionizing radiation field than young O- or B-type stars. These high-energy photons create an extensive partially ionized zone from which low-ionization emission lines, such as [N ii], [S ii] and [O i] originate.

To be sure that no hidden AGN is located in the starburst nuclei of our sample, we compare in Fig. 9 two ratios of low-excitation emission lines, that of [S ii]/Hα and that of [N ii]/Hα. In the presence of a harder ionizing spectrum, both ratios should increase and a correlation would appear. One can clearly see that there is no such relation between the two ratios, neither for the nuclear starbursts nor for the extranuclear ones, which are well mixed in this diagram. In fact, the mean value of [S ii]/Hα is nearly identical for starburst nuclei ($\sim$ 0.20) and extranuclear Hii regions ($\sim$ 0.21). The presence of a weak AGN in the nuclei of our starburst galaxies is also excluded because of the weakness of [O i]λ6300 in their spectrum: only $\sim$ 25% of our nuclear spectra show this emission line with intensities similar to those observed in normal Hii regions (Veilleux & Osterbrock 1987).

Alternative explanations, like collisional excitation by shocks (Kennicutt, Keel & Blaha 1989) or very hot O type stars in metal-rich environments (Fillipenko & Terlevich 1992, Shields 1992), have been suggested as ionization sources to account for the excess of nitrogen emission in galactic nuclei. However, both suggestions fail to reproduce our observations, because they also imply an increase of other low-ionization emission lines like [S ii] and [O i].

We have investigated whether the impact of dust on the thermal properties of Hii regions would provide a better explanation. The dust content in our sample is not negligible since all our galaxies are IRAS sources (one of our selection criteria). Calculations by Shields & Kennicutt (1995) indicate that the influence of dust on the emergent optical spectrum of Hii regions can be quite appreciable in high-metallicity ($Z > Z_{\odot}$) environments, as is the case in many galactic nuclei. In Fig. 1, we compare our data to the results of the photoionization model of Shields & Kennicutt (1995) which incorporates the effects of dust and is calculated for a stellar effective temperature of 45 000 K. The predicted line strengths do not provide a good match for all the observations in our starburst nuclei. The model accounts reasonably well for the [N ii]/Hα ratios observed in high metallicity ([O iii]/H$\beta \leq 0.5$) nuclei and for regions very close to the transition limit between Hii and LINERs, but this appears to be accidental, since the predicted [S ii]/Hα ratio does not match our observations. These theoretical results might simply be the consequence of the selective initial element abundances, since Shields & Kennicutt (1995) arbitrarily assumed an enhancement of nitrogen abundance, with a secondary component scaling as Z^2, while other elements are in solar proportions. The results of the photoionization model of Shields & Kennicutt (1995) might thus follow from this selective abondance introduced *ad hoc* in the model.

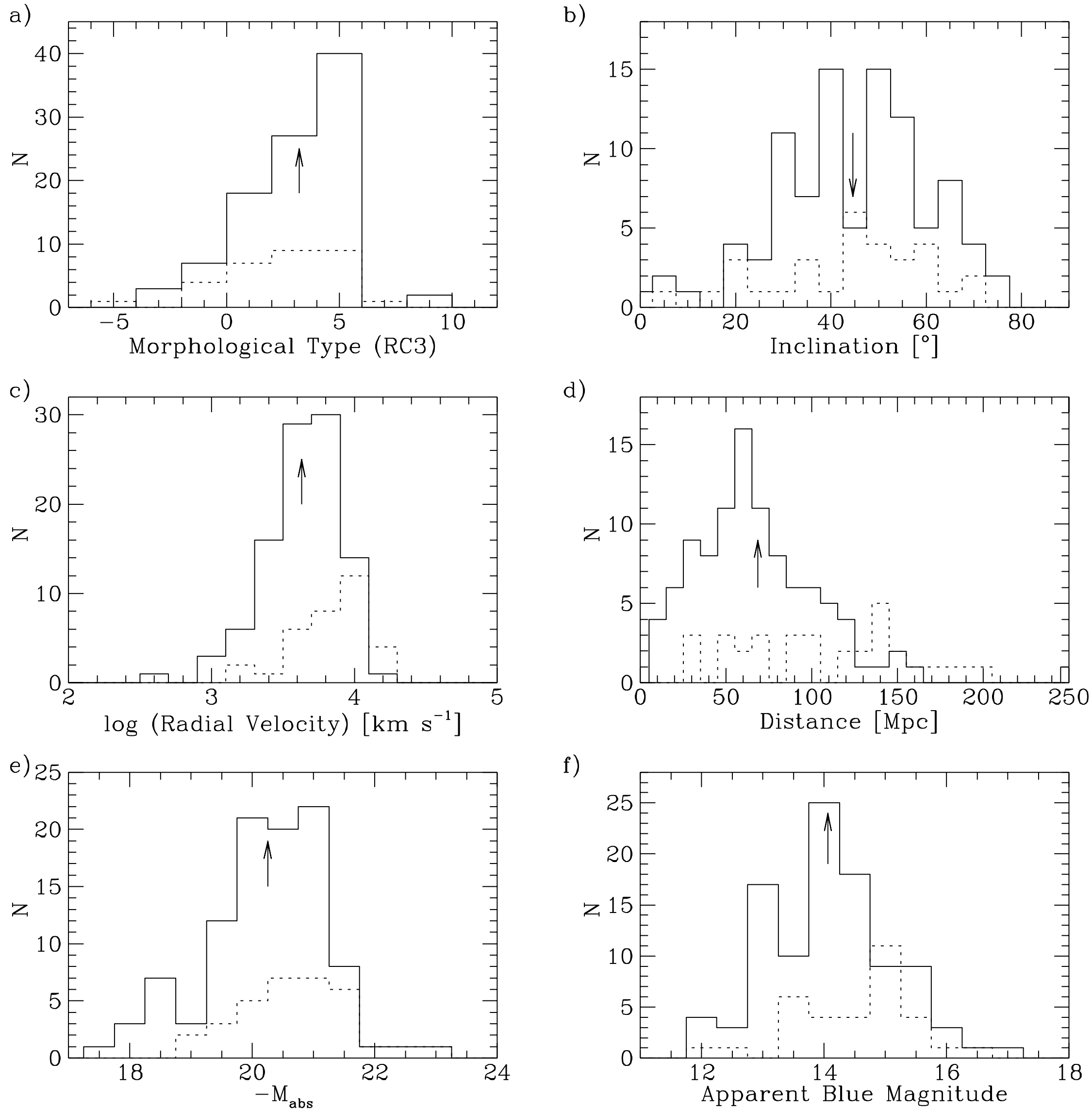

Fig. 10. Distribution of a) morphological type from RC3, b) inclination, c) heliocentric radial velocity, d) distance, e) absolute blue magnitude and f) apparent blue magnitude for SBNGs (*solid line*) and AGNs (*dotted line*). Mean values are indicated by vertical arrows

An enhancement of nitrogen in starburst nuclei is certainly the most reliable explanation to account for the moderate excess of nitrogen emission in our sample of galaxies. Such selective chemical enrichment of nitrogen has been observed in the interstellar medium of some nearby starburst galaxies, like NGC 5253 (Walsh & Roy 1989, Kobulnicky et al. 1997) where N-enriched regions are found in the vicinity of young starbursts with a large population of massive Wolf-Rayet stars (Schaerer et al. 1997). Moreover, chemical evolution models of galaxies (e.g. Marconi, Matteucci & Tosi 1994) predict an enhancement of nitrogen abundance after a succession of short and intense bursts of star formation, which has certainly been the case in starburst nuclei (Coziol 1996).

6. Global properties of SBNGs

6.1. Morphological types, distances, magnitudes and environment

The global properties of our sample of SBNGs are displayed in Fig. 10, which presents the distribution of morphological types (according to RC3), inclinations, heliocentric radial velocities, distances, blue apparent and absolute magnitudes of the galaxies, using the values tabulated in Tables 1 and 4. In these diagrams, we show

the global properties of SBNGs after removing the five HII galaxies and galaxies with ambiguous nuclear spectral classification. The global properties of AGNs (Seyfert 1 and 2, LINERs) are also shown for comparison.

The mean inclination of the galaxies is $\sim 45\,°\pm16$, both for SBNGs and AGNs. This value is comparable to that derived for barred galaxies with HII nuclei (Ho, Filippenko & Sargent 1997b). The heliocentric radial velocity of SBNGs is predominantly ($\sim$ 93%) lower than or equal to 10,000 km s^{-1} with mean values around 4300 and 7000 km s^{-1} for SBNGs and AGNs respectively. The SBNGs are located at a mean distance of 68$\pm$38 Mpc, slightly farther than nearby HII nuclei ($\sim$ 22 Mpc; Ho, Filippenko & Sargent 1997b). The mean distance derived for the AGNs is 107$\pm$50 Mpc. The mean value of the apparent blue magnitude is 14, with a large proportion ($\sim$ 90%) of giant spiral galaxies ($M_{\rm abs} \leq -19.5$). The mean value of the absolute magnitude (~ -20.2) is identical for our sample of SBNGs and for nearby HII nuclei (Ho, Filippenko & Sargent 1997b).

The SBNGs are equally distributed among early-type (S0-a to Sb; 55%) and late-type (Sbc to Sm; 42%) galaxies with only 3% elliptical galaxies as is expected in a sample of starburst galaxies. In fact, the proportion of SBNGs increases with the morphological type and reaches a maximum of 40% for Sbc/Sc galaxies. The distribution of AGNs is on the contrary more uniform from S0 to Sc. One can also note the deficiency of SBNGs with morphological types later than Sc, which confirms the low contamination of our sample by low-luminosity blue compact and irregular HII galaxies.

Coziol, Barth & Demers (1995) found a majority of early-type galaxies among their sample of SBNGs, but this result should be considered with caution because only 39% of their galaxies are morphologically classified. On the contrary, Ho, Filippenko & Sargent (1997b) found a majority of late-type galaxies (62% of Sc-Sm) among their sample of HII nuclei. They note however that this effect is pronounced in barred galaxies (65%) whereas unbarred galaxies with HII nuclei are equally divided between early and late types. This may explain the relatively high frequency of Sc galaxies found in our sample of SBNGs since all our galaxies are barred.

One of the most popular ideas for explaining powerful starbursts is that they must occur preferentially within galaxies undergoing gravitational interactions. We thus performed an analysis of environment and level of interaction for all our galaxies using CCD images (Contini 1996). We found that the majority (62%) of SBNGs are isolated galaxies. Only two galaxies (Mrk 617 and 960) are advanced mergers, 6% of the galaxies belong to close pairs (projected distance $\leq 1'$) and 23% to wide pairs (projected distance $\leq 15'$ and $\Delta V \leq 300$ km s^{-1}). More than half of the SBNGs do not show any sign of past or present gravitational interaction. Asymmetries in the bar or spiral arms are observed in only 32% of the galaxies; among them, 12% have multiple bright knots along the bar. This does not indicate that bars are necessary for triggering starbursts in the absence of interactions; other samples of (barred *and* unbarred) SBNGs (Coziol et al. 1997b) and HII galaxies (Telles & Terlevich 1995) have also been found to contain a low proportion ($\sim$ 20 to 25%) of interacting galaxies. Interactions are more frequent among luminous infrared galaxies. The level of interactions increases with the FIR luminosity, the proportion of mergers reaching a maximum among ultra-luminous infrared galaxies (Veilleux et al. 1995).

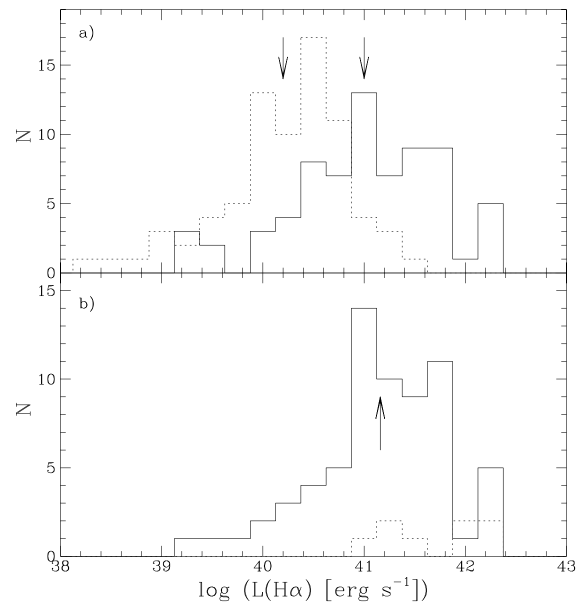

Fig. 11. a) Distribution of reddening-corrected Hα luminosity for individual nuclear (*solid line*) and extranuclear HII region (*dotted line*). b) Distribution of total (nuclear and extranuclear) reddening-corrected Hα luminosity for the SBNGs (*solid line*) and AGNs (*dotted line*). Mean values are indicated by vertical arrows

6.2. Hα luminosity

In this section and the next, we compare the distribution of the Hα and FIR luminosities of our sample of SBNGs with those derived for other samples of starburst galaxies. A more detailed and quantitative discussion on the relation between Hα, blue and FIR luminosities, and on the distribution of Hα equivalent widths in terms of star formation history and age of the starbursts is given in Contini, Considère & Davoust (in preparation).

It appears clearly in Fig. 11a that the average Hα luminosity [log(L(Hα)/erg s^{-1})] is higher (by a factor $\sim$ 10) in starburst nuclei (41.0$\pm$0.7) than in extranuclear HII regions (40.2$\pm$0.6). However, the Hα luminosity of the HII regions, which are mainly located along

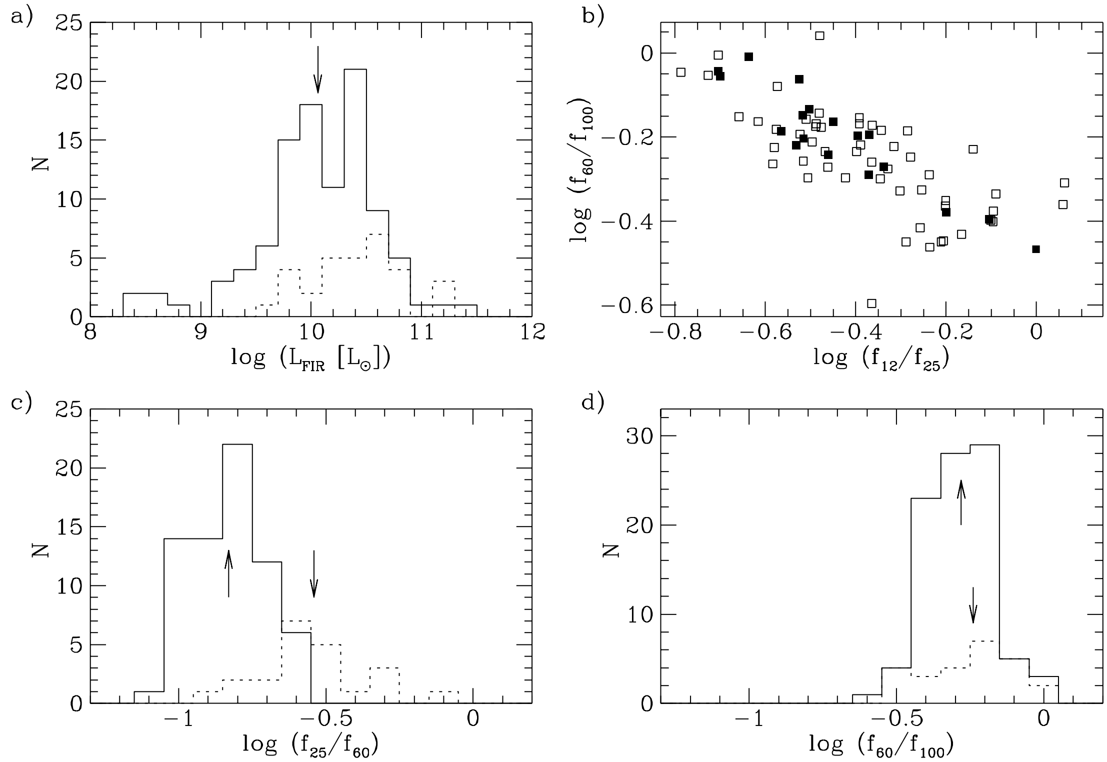

Fig. 12. a) Distribution of total FIR luminosity for the SBNGs (*solid line*) and AGNs (*dotted line*). b) IRAS color-color diagram for SBNGs (*open squares*) and AGNs (*filled squares*), c) and d) Distributions of f_{25}/f_{60} and f_{60}/f_{100} IRAS colors for SBNGs (*solid line*) and AGNs (*dotted line*). Mean values are indicated by vertical arrows

the bar of our galaxies, is higher than that of typical disk HII regions (39.5; Kennicutt, Keel & Blaha 1989). The Hα luminosities estimated in our starburst nuclei are typical of starburst galaxies (40.7; Balzano 1983). They are clearly higher than in nearby HII nuclei (39.2; Ho, Filippenko & Sargent 1997a) but slightly lower than in starbursts in luminous infrared galaxies (42.0; Veilleux et al. 1995). Contrary to what occurs in nearby HII nuclei (Ho, Filippenko & Sargent 1997a), we do not find any significant difference between the total Hα luminosities of early-type (41.3±0.4) and late-type (41.0±0.7) SBNGs.

In terms of Hα luminosity, our sample of SBNGs is thus intermediate between nearby HII nuclei and luminous infrared galaxies. These luminosities are typical of starburst galaxies and comparable to other samples of SBNGs (i.e. Coziol et al. 1994).

As shown in Fig. 11b, the total (nuclear and extranuclear) Hα luminosity derived for SBNGs (41.2±0.6) is slightly lower than that derived for AGNs (41.7± 0.5). These luminosities are very close to those observed in other samples of Seyfert galaxies (∼ 42.0; Dahari & De Robertis 1988, Veilleux et al. 1995).

6.3. FIR properties

We computed the FIR luminosities of the galaxies from the IRAS flux densities at 60 and 100 μm (Table 1) using the following relation which approximates well the total FIR luminosity between 42 and 122 μm (Helou et al. 1988)

$$\log(L_{\rm FIR}) = 5.5378 + 2\log(D) + \log(2.58 f_{60} + f_{100}) \qquad (1)$$

where the flux densities at 60 and 100 μm are expressed in Janskys, D is the distance of the galaxy in Mpc and $L_{\rm FIR}$ is the FIR luminosity in solar units.

The distribution of FIR luminosities [$\log(\rm L_{FIR}/L_\odot)$] is shown in Fig. 12a. Our sample of SBNGs has moderate FIR luminosities (10.1±0.5), slightly higher than those observed in samples of HII nuclei (∼ 9.4) and HII galaxies (∼ 8.9), similar to other samples of SBNGs (∼ 9.9) (see Coziol 1996 and references therein) but rather low compared to samples of luminous (∼ 11) or ultra-luminous (∼ 12) infrared galaxies (Veilleux et al. 1995). There is no significant difference between the average FIR luminosity of the SBNGs and AGNs (10.4±0.4). The AGNs in our sample follow the trend observed in infrared-bright galaxies, their proportion increases with FIR luminosity and reaches a maximum of 62% for $\log(L_{\rm FIR}/L_\odot) \geq 12$ (Veilleux et al. 1995).

We did not use the fluxes at 12 and 25 μm to compute the FIR luminosities, because of the strong contribution of non-thermal radiation to dust heating at these wavelengths. This well-known phenomenon (e.g. Miley, Neugebauer & Soifer 1985, de Grijp et al. 1985) is illustrated in Figs. 12c,d where we show the distribution of the two IRAS colors, f_{25}/f_{60} and f_{60}/f_{100}, for both SBNGs and AGNs. While no difference is seen in the distribution of f_{60}/f_{100} (mean value ~ 0.55) for AGNs and starburst galaxies, a clear excess of emission at 25 μm is observed for AGNs $[\log(f_{25}/f_{60}) = -0.5 \pm 0.2]$ when compared to SBNGs $[\log(f_{25}/f_{60}) = -0.8 \pm 0.1]$. This indicates that the infrared emission at short wavelengths (12 and 25 μm) is mainly due to a "warm dust" component heated by the non-thermal ionizing radiation from AGNs. Figure 12b also shows that, regardless of the spectral classification, there is a clear tendency for galaxies with "warmer" 60/100 colors to have "cooler" 12/25 colors, illustrating the need for a multicomponent model to describe the nature of IRAS infrared emission (e.g. Helou 1986). Such a model requires the presence of a "warm dust" component of infrared emission associated with star formation regions, and a "cool dust" component associated with the neutral interstellar medium.

7. Summary and conclusion

We presented optical long-slit spectroscopic observations of 105 barred Markarian IRAS galaxies. These observations were mainly used to assign a spectral type (nuclear starburst, HII region, Seyfert 1 or 2) to each emission-line region along the slit, and to define a homogeneous sample of starburst nuclei and extranuclear HII regions.

Our selection criteria (UV excess, FIR emission and barred morphology) have been very efficient for selecting star-forming galaxies, since our sample of 221 emission-line regions includes 82% nuclear or extranuclear starbursts. The contamination by AGNs is low (9%), with 13 Seyfert 1 and 8 Seyfert 2 nuclei. The remainder are objects with ambiguous classification between HII and LINER.

Our sample of star-forming galaxies contains only 5 HII galaxies, characterized by a high excitation parameter, equivalent to a low metallicity. In fact, our sample is strongly biased towards energetic starbursts located in the nuclear or extranuclear regions of more massive and chemically evolved galaxies than HII galaxies. Three Wolf-Rayet galaxies (Mrk 52, 710 and 712) are also included in our sample.

We first compared the physical properties of the starburst nuclei to those of extranuclear HII regions distributed along the bar and to those of typical disk HII regions (Kennicutt, Keel & Blaha 1989). The amount of reddening, and hence the dust content, increases towards the nucleus of the galaxy. The same trend is also observed for the Hα luminosity; the highest star formation rates are observed in the nuclei of the galaxies. We also found that the mean Hα luminosity of the bar HII regions is higher than that of typical disk HII regions, probably because we are dealing with starburst galaxies. We did not observe any significant variation of the electron density in the nuclei and bar HII regions, but the measured values are higher (by a factor of about 3) than in typical disk HII regions. The excitation parameter, [O III]/Hβ, generally decreases from the center outwards, reflecting the negative metallicity gradient observed in barred (Considère, Contini & Davoust, in preparation) and ordinary spiral galaxies.

We investigated different mechanisms for explaining the excess of nitrogen emission observed in starburst nuclei, which however is low compared to that estimated in nearby HII nuclei and other SBNGs. There is no evidence for the presence of a weak hidden AGN in the nuclei of our starburst galaxies, as suggested by Kennicutt, Keel & Blaha (1989) for explaining the excess of nitrogen in other samples of such galaxies. The most likely explanation is a selective enrichment of nitrogen in the nuclei of galaxies, following a succession of short and intense bursts of star formation.

The properties of our sample of SBNGs are very much like those of other samples of SBNGs (Coziol et al. 1997b) and starburst galaxies (Balzano 1983) located at a redshift of $\sim 0.01 - 0.02$ and with nearly the same Hα and FIR luminosities. The host galaxies are distributed equally among early- and late-type giant spirals with a slight preference for Sbc/Sc types in our sample, a selection effect caused by the presence of a bar. The majority of SBNGs are isolated with no sign of gravitational interaction, contrary to the opinion that starbursts in massive galaxies are produced by gravitational interactions. This result suggests that, in the majority of spiral galaxies, bursts of star formation may depend on internal mechanisms, rather than on gravitational interactions.

SBNGs are intermediate between low-mass irregular HII galaxies (Terlevich et al. 1991) or nearby HII nuclei (Ho, Filippenko & Sargent 1997a) and luminous or ultraluminous infrared galaxies (Veilleux et al. 1995). The former are closer and intrinsicaly less luminous in Hα and in the FIR whereas the latter are farther and more luminous, both in Hα and FIR, with a high proportion of interacting galaxies.

This spectrophotometric dataset on starbursts has been used to determine the age and star formation rate of the starbursts (Contini, Davoust & Considère, in preparation) and, together with millimetric observations of the molecular gas, to establish the presence of molecular gas outflows in the nuclei of barred starburst galaxies (Contini et al. 1997a). New spectrophotometric observations of a subset of this sample, with better signal-to-noise ratio and including the [O II]λ3727 emission line, have been used to derive the metallicity of the nebular gas and its gradient along the bar of the galaxies (Considère,

Contini & Davoust, in preparation), and have revealed yet another Wolf-Rayet galaxy.

The detailed spectroscopic analysis of some galaxies of the sample (Mrk 710, 712 and 799), combined with CCD imaging and observations of molecular clouds and atomic hydrogen has given rise to new results concerning the population of massive stars and the starburst properties in Wolf-Rayet galaxies (Contini et al. 1997b). The analysis of the optical and CO velocity fields of Mrk 799 is in progress.

The link between the morphological and dynamical parameters of the bar (bar strength and relative length) and the starburst activity in the center of barred spiral galaxies has been investigated by Chapelon, Contini & Davoust (in preparation).

Finally, our data have been used together with another sample of starburst galaxies to shed new light on the formation and chemical evolution of galaxies, by showing that SBNGs are still in the process of formation because of their underabundance in oxygen with respect to "normal" spiral galaxies (Coziol et al. 1997a).

Acknowledgements. Data from the literature were obtained with the Lyon Meudon Extragalactic database (LEDA), supplied by the LEDA team at CRAL-Observatoire de Lyon (France). We thank Roger Coziol for helpful comments on the manuscript and the staff of Observatoire de Haute-Provence for assistance at the telescope.

References

Baldwin J.A., Phillips M.M., Terlevich R., 1981, PASP 93, 5
Balzano V.A., 1983, ApJ 268. 602
Bicay M.D., Kojoian G., Seal J., Dickinson D.F., Malkan M.A. 1995, ApJ 98, 369
Buta R., Williams K.L., 1995, AJ 109, 543
Conti P.S., 1991, ApJ 377, 115
Contini T., 1996, Ph.D. thesis, Université Paul Sabatier, Toulouse, France
Contini T., Davoust E., Considère S., 1995, A&A 303, 440 (paper I)
Contini T., Wozniak H., Considère S., Davoust E., 1997a, A&A 318, L51
Contini T., Wozniak H., Considère S., Davoust E., 1997b, A&A 324, 41 (paper II)
Coziol R., 1996, A&A 309, 345
Coziol R., Barth C.S., Demers S., 1995, MNRAS 276, 1245
Coziol R., Contini T., Davoust E., Considère S., 1997a, ApJ 481, L67
Coziol R., Demers S., Barnéoud R., Peña M., 1997b, AJ 113, 1548
Coziol R., Demers S., Peña M., Barnéoud R., 1994, AJ 108, 405
Dahari O., De Robertis M.M., 1988, ApJS 67, 249
de Grijp M.H.K., Miley G.K., Lub J., de Jong T., 1985, Nature 314, 240
de Vaucouleurs G., de Vaucouleurs A., Corwin H.G., Buta R.J., Paturel G., Fouqué P., 1991, *Third Reference Catalog of Bright Galaxies*, New-York, Springer-Verlag
Filippenko A.V., Terlevich R., 1992, ApJ 397, L79
French H.B., 1980, ApJ 240, 41
Heckman T.M., 1980, A&A 87, 142
Helou G., 1986, ApJ 311, L33
Helou G., Khan I.R., Malek L., Boehmer L., 1988, ApJS 68, 151
Ho L.C., Filippenko A.V., Sargent W.L.W., 1997a, ApJ 487, 579
Ho L.C., Filippenko A.V., Sargent W.L.W., 1997b, ApJ 487, 591
Keel W.C., 1983, ApJ 296, 466
Kennicutt R.C, Keel W.C., Blaha C.A., 1989, AJ 97, 1022
Kobulnicky H.A., Skillman E.D., Roy J-R., Walsh J.R., Rosa M.R., 1997, ApJ 477, 679
Leitherer C., Heckman T.M., 1995, ApJS 96, 9
Lemaître G., Kohler D., Lacroix D., Meunier J-P., Vin A., 1990, A&A 228, 540
Marconi G., Matteucci F., Tosi M., 1994, MNRAS 270, 35
Massey P., Strobel K., Barnes J.V., Anderson E., 1988, ApJ 328, 315
Mazzarella J.M., Balzano V., 1986, ApJS 62, 751
Mazzarella J.M., Boroson T.A., 1993, ApJS 85, 27
McCall M.L., Rybski P.M., Shields G.A., 1985, ApJS 57, 1
Miley G.K., Neugebauer G., Soifer B.T., 1985, ApJ 293, L11
Oke J.B., Gunn J.E., 1983, ApJ 266, 713
Osterbrock D.E., 1989, *Astrophysics of Gaseous Nebulae and Active Galactic Nuclei*. University Science Books, Mill Valley
Rees M.J., 1984, ARA&A 22, 471
Schaerer D., Contini T., Kunth D., Meynet G., 1997, ApJ 481, L75
Shields J.C., 1992, ApJ 399, L27
Shields J.C., Kennicutt R.C., 1995, ApJ 454, 807
Shuder J.M., Osterbrock D.E., 1981, ApJ 250, 55
Stauffer J.P., 1982, ApJS 50, 517
Telles E., Terlevich R., 1995, MNRAS 275, 1
Terlevich R., Melnick J., Masegosa J., Moles M., Copetti M.V.F., 1991, A&AS 91, 285
Veilleux S., Kim D-C., Sanders D.B., Mazzarella J.M., Soifer B.T., 1995, ApJS 98, 171
Veilleux S., Osterbrock D.E., 1987, ApJS 63, 295
Walsh J.R., Roy J-R., 1989, MNRAS 239, 297

This article was processed by the author using Springer-Verlag LaTeX A&A style file *L-AA* version 3.

Table 1. Global properties of the sample of barred Markarian galaxies

(1) Markarian number
(2) Right ascension (equinox 1950) in hours
(3) Declination (equinox 1950) in degrees
(4) Other name
(5) Morphological type from RC3
(6) Ring
(7) Multiple system
(8) Code for morphological type (RC3)
(9) Inclination angle in degrees (angle between the plane of the sky and the galactic disk)
(10) Heliocentric radial velocity (in km s^{-1})
(11) Apparent blue magnitude
(12) Absolute blue magnitude
(13-20) Far-infrared flux densities and associated quality codes for the 4 IRAS bands (from Bicay et al. 1995):

- (13-14) Quality (q_{12}) and flux density (F_{12}, in Jy) at 12 μm
- (15-16) Quality (q_{25}) and flux density (F_{25}, in Jy) at 25 μm
- (17-18) Quality (q_{60}) and flux density (F_{60}, in Jy) at 60 μm
- (19-20) Quality (q_{100}) and flux density (F_{100}, in Jy) at 100 μm

Mrk	$\alpha(1950)$	$\delta(1950)$	Name	Morph.	R	M	Type	i	$V_\odot$	m_B	M_{abs}	q_{12}	F_{12}	q_{25}	F_{25}	q_{60}	F_{60}	q_{100}	F_{100}
	[h]	[°]						[°]	[km s^{-1}]				[Jy]		[Jy]		[Jy]		[Jy]
(1)	(2)	(3)	(4)	(5)	(6)	(7)	(8)	(9)	(10)	(11)	(12)	(13)	(14)	(15)	(16)	(17)	(18)	(19)	(20)
1	1.22208	32.8258	NGC 449	SBbc			4.0	53.9	4822	15.01	-19.60	1	1.8870	3	0.8648	3	2.5310	2	2.9210
2	1.86547	36.6722	UGC 1385	SBab			2.0	30.9	5576	13.91	-20.99	3	0.2109	3	0.9621	2	5.4860	2	7.7800
4	6.35769	74.3314	UGC 3460	SBc			5.2	62.7	5255	14.70	-19.73	3	0.1403	3	0.2665	3	2.3400	2	4.1390
10	7.71872	61.0564	UGC 4013	SBbc	R		4.2	68.9	8749	13.39	-22.76	3	0.1396	3	0.2206	3	0.8130	2	1.9480
12	7.74472	74.4850	UGC 4028	SBc			5.2	37.9	3954	13.10	-21.13	3	0.1943	3	0.3092	3	3.2320	2	7.4740
13	7.86578	60.4381	IC 2209	SBbc			4.4	32.2	1428	14.31	-17.77	1	0.1270	1	0.0928	3	0.4082	1	1.3860
21	9.74931	58.2036	UGC 5243	SBbc			3.5	49.3	8460	14.95	-20.80	1	0.0985	2	0.1087	3	0.4829	2	1.2970
31	10.27333	57.6722	NGC 3188	SBbc	R	M	3.7	21.9	7805	14.60	-20.35	1	0.0974	1	0.0957	3	0.5345	2	1.2500
38	11.25717	54.0222	MCG 9-19- 34	SBab		M	2.0	63.3	10774	15.41	-21.00	1	0.1241	1	0.1128	3	0.5551	2	1.1420
39	11.25831	54.0239	MCG 9-19- 35	SBab		M	2.0	55.2	10893	16.93	-19.42	1	0.1241	1	0.1128	3	0.5551	2	1.1420
42	11.85147	46.4889	MCG 8-22- 28	SBc	R		5.0	37.4	7200	15.46	-19.81	1	0.0987	1	0.1394	3	0.3172	1	0.9099
52	12.38581	0.8500	NGC 4385	SBa			0.8	58.2	2141	13.16	-19.33	3	0.2802	3	1.0500	3	4.7260	2	5.6800
58	12.94456	27.9153	MCG 5-31- 57	SBab			2.4	30.0	5526	15.16	-19.50	1	0.1053	1	0.0945	3	0.3773	2	0.5773
78	7.63219	65.2953	Mrk 78	SB			...	58.6	11273	15.22	-20.70	3	0.1278	3	0.5546	3	1.1100	2	1.1320
79	7.64636	49.9297	UGC 3973	SBb			2.7	3.8	6645	13.57	-21.64	3	0.3062	3	0.7625	3	1.5030	2	2.3630
86	8.16197	46.1425	NGC 2537	SBc			6.0	32.0	447	12.21	-18.67	2	0.1475	3	0.3270	3	3.2360	2	6.4480
87	8.26531	74.1481	NGC 2544	SBab	R		1.8	44.7	3503	13.87	-20.14	1	0.1018	2	0.1176	3	1.3090	2	3.6710
90	8.43769	52.8647	UGC 4438	SBc			5.0	29.2	4270	14.04	-20.17	1	0.0982	2	0.1560	3	0.9538	2	2.1580
109	9.31812	47.4581	MCG 8-17- 86	SBm			9.0	49.9	9100	15.87	-19.96	1	0.0944	1	0.1708	3	0.6596	2	1.0710
114	9.44356	56.0722	UGC 5055	SBbc			4.4	35.4	7534	14.30	-21.12	2	0.0826	3	0.1657	3	1.4920	2	3.1750
122	9.72069	73.1972	NGC 2963	SBb			2.7	65.5	6553	14.33	-21.15	1	0.1216	3	0.1268	3	1.1380	2	3.1900
133	9.96444	72.3647	NGC 3066	SBbc			4.2	12.3	2082	13.54	-19.25	3	0.1652	3	0.5420	3	3.0870	2	5.5760
141	10.26075	64.2206	MCG 11-13- 18	E			-5.0	...	12237	15.41	-20.70	2	0.1279	2	0.1624	3	0.7408	2	1.8380
152	10.76500	50.3036	MCG 8-20- 28	SBab			2.0	69.4	6910	14.95	-20.58	1	0.1219	2	0.1886	3	0.7619	2	1.0060
161	10.98536	45.4964	UGC 6103	SBbc			4.0	52.7	5985	13.99	-20.96	2	0.1246	3	0.3998	3	2.2720	2	4.4970
179	11.51439	62.1647	NGC 3725	SBc			5.0	39.8	3324	13.80	-19.91	2	0.0915	3	0.1655	3	0.9042	2	2.3570
185	11.64333	47.9703	NGC 3811	SBc			5.5	42.7	3103	12.90	-20.61	3	0.1986	3	0.1733	3	2.3950	2	5.4970
188	11.74831	56.2492	NGC 3888	SBc			5.2	39.7	2407	12.71	-20.31	3	0.3621	3	0.4515	3	4.5760	2	11.5200
213	12.48406	58.2403	NGC 4500	SBa	R		1.2	49.1	2922	13.10	-20.40	3	0.2786	3	0.6134	3	3.9360	2	6.0060
236	12.97167	61.9242	MCG 10-19- 11	SBab			2.0	55.2	15000	16.60	-19.90	1	0.0636	1	0.0963	3	0.1733	1	0.6415
257	13.42044	55.7444	NGC 5164	SBbc		M	3.7	25.1	7023	14.59	-20.40	1	0.0486	1	0.0935	3	0.3395	2	1.2250
262	13.49039	75.8236	Mrk 262	SB			...	...	9000	15.75	-19.40	1	0.2500	1	0.2500	3	0.9610	3	1.8500
264	13.53647	52.1453	Mrk 264	SBc			4.0	...	18817	16.51	-20.00	1	0.0850	1	0.1132	3	0.7645	1	2.4570
271	13.66311	55.9219	NGC 5278	SBbc		M	4.2	43.5	7536	13.72	-21.73	3	0.1888	3	0.1892	3	1.5250	2	4.4730
281	13.91683	42.0889	NGC 5383	SBbc			3.8	36.1	2249	12.10	-20.73	3	0.3524	2	0.6853	3	4.8910	2	13.7500
288	14.84728	74.0278	MCG 12-14- 13	SBc			5.0	68.8	7500	15.70	-20.11	1	0.0762	1	0.0597	3	0.3319	2	0.7404

Mrk	α(1950)	δ(1950)	Name	Morph.	R	M	Type	i	$V_\odot$	m_B	M_{abs}	q_{12}	F_{12}	q_{25}	F_{25}	q_{60}	F_{60}	q_{100}	F_{100}
	[h]	[°]						[°]	[km s^{-1}]				[Jy]		[Jy]		[Jy]		[Jy]
(1)	(2)	(3)	(4)	(5)	(6)	(7)	(8)	(9)	(10)	(11)	(12)	(13)	(14)	(15)	(16)	(17)	(18)	(19)	(20)
291	15.88169	19.3389	Mrk 291	SBbc			3.5	47.4	10531	15.83	-20.43	1	0.0662	1	0.0884	3	0.3368	1	0.9756
300	16.06689	18.3164	IC 1189	SBa	R		1.4	57.5	11684	15.38	-21.27	1	0.0844	1	0.1007	3	0.6593	1	2.1310
306	22.49067	19.4353	UGC 12066	SBc		M	5.0	52.3	5608	14.39	-20.57	1	0.0954	1	0.1738	3	1.1030	2	2.3720
307	22.55872	20.0647	NGC 7316	SBc			5.5	37.0	5558	13.63	-21.23	2	0.1518	3	0.1887	3	1.7800	2	4.2320
311	22.93480	14.9019	IC 1461	SBc			6.0	...	9130	14.95	-20.85	2	0.1027	3	0.2381	3	1.8170	2	3.3050
313	22.99217	15.6964	NGC 7465	SBO			-1.7	59.3	1963	13.32	-19.24	1	0.3235	1	0.4937	3	3.7990	2	7.3950
319	23.26953	24.9575	UGC 12490	SBab			2.2	54.6	8077	14.20	-21.58	3	0.2211	3	0.5418	3	4.2660	2	7.0620
323	23.29860	27.0406	NGC 7624	SBc			5.5	43.7	4255	13.84	-20.47	3	0.2739	3	0.3459	3	3.1610	2	7.9110
326	23.42667	23.2547	NGC 7677	SBbc			3.7	50.1	3545	13.91	-20.02	3	0.2318	3	0.7145	3	3.9560	2	5.9150
332	23.94769	20.4717	NGC 7798	SBc			4.5	24.3	2406	12.97	-19.98	3	0.3598	3	0.6212	3	4.8710	2	9.4930
339	0.36872	14.5453	UGC 233	SBbc			4.0	...	5281	14.53	-19.80	1	0.1544	2	0.1506	3	0.5378	2	1.3720
353	1.00972	22.0739	NGC 354	SBc			5.0	57.5	4671	14.28	-20.21	3	0.2325	3	0.5740	3	3.8770	2	5.7130
358	1.39586	31.3536	MCG 5- 4- 59	SBc			4.8	42.4	13553	15.06	-21.73	2	0.0871	1	0.1416	3	0.3178	1	1.2570
359	1.41392	18.9186	UGC 1032	SBab			2.0	36.8	5077	14.17	-20.38	2	0.1192	3	0.4376	3	1.1320	2	1.7400
373	6.84519	50.4167	Mrk 373	SBc			4.0	...	5939	15.28	-19.40	2	0.1028	3	0.3164	3	1.8260	2	2.6880
374	6.92608	54.2647	MCG 9-12- 16	SBab			2.0	70.2	12999	14.89	-22.29	2	0.1123	3	0.1940	3	0.2658	1	0.6811
382	7.86756	39.3186	MCG 7-17- 1	SBc			5.5	30.1	10166	15.06	-21.05	1	0.1469	1	0.2431	3	0.2154	1	0.7357
384	8.00233	23.5333	NGC 2512	SBb			2.7	50.8	4702	13.86	-20.66	2	0.1523	3	0.5839	3	3.7130	2	6.8130
386	8.28114	22.1853	NGC 2565	SBbc	R	M	4.2	66.5	3590	13.34	-20.71	1	0.0926	1	0.1976	3	0.6903	2	2.1200
401	9.45542	29.7592	NGC 2893	SBab	R		2.0	26.7	1699	13.87	-18.26	3	0.1687	3	0.5619	3	2.5730	2	4.0130
412	9.91792	32.4778	MCG 5-24- 5	SBm			10.0	63.7	4518	15.25	-19.17	1	0.0974	1	0.2327	3	0.5163	1	0.6981
446	12.79553	33.4297	NGC 4719	SBbc			4.2	40.4	7091	13.93	-21.31	2	0.0982	3	0.2884	3	1.4950	2	2.5680
471	14.34636	33.0769	UGC 9214	SBb			3.2	51.4	10261	14.54	-21.59	2	0.1138	1	0.1824	3	0.7648	2	2.2520
474	14.55167	48.8797	NGC 5683	SBO-a	R		0.0	49.9	10840	15.71	-20.51	1	0.2500	1	0.2500	3	0.4710	3	1.3400
479	14.87792	18.2375	IC 1076	SBc			4.7	60.2	6070	14.19	-20.92	2	0.1065	2	0.1692	3	1.7220	2	3.8650
489	15.71008	41.2500	NGC 5992	SBb		M	2.7	51.7	9560	14.31	-21.72	1	0.1097	1	0.2197	3	1.8090	2	4.6900
493	15.95461	35.1703	UGC 10120	SBb			3.2	13.6	9438	14.98	-20.88	2	0.0881	3	0.1918	3	0.6937	2	1.2940
527	23.17794	6.0489	NGC 7518	SBb	R		3.0	53.6	3536	14.26	-19.60	1	0.0975	1	0.3830	3	4.2030	2	7.6670
529	23.19661	-3.0000	NGC 7532	SBO-a			-1.0	71.1	3535	13.85	-19.83	2	0.1184	2	0.2283	3	1.6890	2	2.5860
533	23.42345	8.5017	NGC 7674	SBc		M	4.5	24.4	8766	13.95	-21.74	3	0.6724	3	1.8960	3	5.5880	2	8.1460
534	23.43711	3.2358	NGC 7679	SBa			1.0	57.1	5139	13.38	-21.32	1	0.4984	1	1.4940	2	6.9060	2	10.6600
538	23.56143	1.8783	NGC 7714	SBbc		M	4.4	41.2	2799	12.97	-20.27	3	0.4659	2	2.8500	3	10.3600	2	11.5100
545	0.12183	25.6450	NGC 23	SBb			2.8	47.9	4565	12.82	-21.61	3	0.5230	2	1.0820	3	9.1960	2	15.3400
552	0.47886	8.1997	MCG 1- 2- 18	SBa			1.0	31.9	4351	14.52	-19.65	1	0.2127	3	0.4032	3	3.6010	2	5.3870
565	1.22456	4.0308	IC 89	SBO			-2.0	43.2	5461	13.07	-21.55	1	0.2083	1	0.1388	3	1.4990	2	3.4200
571	1.55719	0.4089	NGC 622	SBbc			3.8	46.0	5159	13.99	-20.56	1	0.1418	1	0.2229	3	1.5070	2	2.6220

Mrk	$\alpha(1950)$	$\delta(1950)$	Name	Morph.	R	M	Type	i	$V_{\odot}$	m_B	M_{abs}	q_{12}	F_{12}	q_{25}	F_{25}	q_{60}	F_{60}	q_{100}	F_{100}
	[h]	[°]						[°]	[km s^{-1}]				[Jy]		[Jy]		[Jy]		[Jy]
(1)	(2)	(3)	(4)	(5)	(6)	(7)	(8)	(9)	(10)	(11)	(12)	(13)	(14)	(15)	(16)	(17)	(18)	(19)	(20)
575	1.76467	12.3642	UGC 1260	SBa			1.0	39.2	5486	13.84	-20.88	1	0.2247	3	0.4908	3	2.7910	2	5.3680
592	2.28542	-0.4856	UGC 1794	SBbc			3.5	37.0	7623	14.24	-21.17	1	0.2094	2	0.2801	3	1.6200	2	2.4100
593	2.39858	11.9289	NGC 927	SBc	R		5.0	2.8	8260	14.59	-20.97	1	0.1744	1	0.3674	3	0.8157	2	2.2850
602	2.95392	2.5733	IC 277	SBc			4.5	36.7	2850	13.86	-19.42	3	0.1658	3	0.6249	3	3.6870	2	5.6020
617	4.52653	-8.6783	NGC 1614	SBbc		M	4.0	30.5	4773	13.60	-20.83	3	1.4410	3	7.2860	2	32.3100	2	32.6900
618	4.56658	-10.4778	MCG -2-12- 45	SBb			2.5	43.4	10619	14.60	-21.20	3	0.3365	3	0.7884	3	2.7060	2	4.2400
620	6.76042	60.9036	NGC 2273	SBa	R		0.7	44.5	1840	12.54	-20.11	3	0.4003	3	1.3620	3	6.0210	2	10.0000
665	13.99173	34.0669	NGC 5421	SBO-a		M	0.0	31.3	7882	14.46	-21.00	1	0.0768	2	0.1405	3	0.7616	2	1.6060
686	14.58907	36.7869	NGC 5695	SBc			5.0	45.7	4223	13.57	-20.60	1	0.1053	2	0.1288	3	0.5655	2	1.7900
691	15.74533	18.0394	NGC 5996	SBc		M	5.0	53.5	3303	13.01	-20.77	3	0.2006	3	0.5308	3	3.9090	2	7.7430
703	8.93653	6.4881	NGC 2718	SBb			3.0	2.0	3842	13.07	-20.75	3	0.2631	3	0.5610	3	3.6690	2	6.9230
708	9.65956	4.9019	NGC 2966	SBc			4.5	70.5	2039	13.79	-18.96	3	0.2526	3	0.7646	3	5.4370	2	7.5640
710	9.86950	9.5089	NGC 3049	SBb	R		3.0	50.6	1493	13.33	-18.49	2	0.1421	3	0.4255	3	2.8180	2	4.2400
712	9.89975	15.8761	UGC 5342	SBbc			3.5	62.9	4550	14.03	-20.38	1	0.0690	2	0.1865	3	0.8528	2	1.6550
718	10.15983	5.1711	UGC 5501	SBc			5.0	2.8	8434	14.37	-21.14	2	0.1398	2	0.2048	3	1.2280	2	3.3140
731	11.16770	9.3289	IC 676	SBO-a			-1.5	49.3	1411	13.12	-18.45	2	0.1876	1	0.8112	3	3.1950	2	4.8800
752	11.83611	2.0175	UGC 6854	SBc			5.0	35.0	6126	14.15	-20.69	1	0.1411	1	0.2362	3	0.7624	2	1.4950
759	12.13461	16.3117	NGC 4152	SBc			4.7	37.6	2163	12.65	-19.95	3	0.2995	2	0.5370	3	4.1160	2	8.7270
766	12.26542	30.0908	NGC 4253	SBab			1.7	22.1	3836	13.71	-20.15	3	0.3855	3	1.2950	3	4.0260	2	4.6580
781	12.85544	9.9803	NGC 4779	SBbc			4.2	31.7	2829	13.19	-19.97	2	0.1363	1	0.4385	3	1.8960	2	4.0290
799	13.98569	59.5694	NGC 5430	SBb			3.0	51.7	2970	12.84	-20.72	3	0.5614	3	1.6280	3	10.4100	2	19.4700
803	14.04136	12.9442	UGC 9002	SBO-a	R	M	0.0	51.0	4101	14.88	-19.14	1	0.1034	1	0.1626	3	0.3945	1	1.4920
804	14.05983	13.0214	MCG 2-36- 39	SBc			5.5	33.2	5285	14.78	-19.80	1	0.0907	1	0.1895	3	0.5951	2	1.4320
814	14.47572	29.4022	NGC 5657	SBb	R		3.0	70.8	3909	14.09	-20.21	2	0.1111	3	0.1534	3	1.6140	2	2.7360
860	15.62194	25.1094	MCG 4-37- 16	SBab		M	2.0	63.3	6869	15.43	-20.02	2	0.1006	3	0.5360	3	2.3650	2	2.6750
861	15.79042	12.5508	IC 1141	SBc			5.0	20.8	4409	14.42	-19.86	2	0.1003	3	0.2319	3	1.3440	2	1.9990
871	16.10432	12.4614	IC 1198	SBc			5.5	60.1	10145	14.88	-21.44	2	0.0964	3	0.3177	3	0.6896	2	0.9707
874	16.18275	60.7092	UGC 10279	SBb		M	3.0	60.0	4128	14.79	-19.58	1	0.0386	2	0.0525	3	0.3951	2	0.7576
898	21.16267	11.4539	UGC 11697	SBbc			4.0	51.6	5136	15.09	-19.83	1	0.1195	1	0.2090	3	0.9468	2	1.1780
917	22.64672	31.9083	UGC 12149	SBa			1.3	21.4	7316	14.59	-20.97	3	0.1856	3	0.6094	3	3.7140	2	5.9460
955	0.58392	0.0058	MCG 0- 2- 94	SBbc			4.0	49.3	10444	14.98	-21.14	1	0.1477	1	0.4131	3	0.9385	2	1.7830
960	0.76800	-12.9894	MCG -2- 3- 19	SBO-a			0.3	50.3	6407	13.91	-21.03	1	0.1178	1	0.2966	3	1.3550	2	1.9690
968	0.97078	-9.4547	MCG -2- 3- 63	SBc	R		4.5	20.6	4489	15.50	-19.70	1	0.1156	1	0.3073	3	0.8189	2	1.8030
984	1.27925	12.1842	UGC 849	SBc			6.3	61.9	14315	14.83	-22.12	1	0.1118	1	0.1960	3	0.5153	2	1.6880
1009	1.79689	35.0369	NGC 688	SBb			3.4	54.6	4143	13.35	-21.00	2	0.1147	2	0.1412	3	1.2860	2	2.7830
1026	2.13061	-10.5553	NGC 848	SBb			3.0	50.4	3957	13.60	-20.38	1	0.1996	2	0.2401	3	1.4380	2	3.2610

Mrk	α(1950)	δ(1950)	Name	Morph.	R	M	Type	i	$V_{\odot}$	m_B	M_{abs}	q_{12}	F_{12}	q_{25}	F_{25}	q_{60}	F_{60}	q_{100}	F_{100}
	[h]	[°]						[°]	[km s^{-1}]				[Jy]		[Jy]		[Jy]		[Jy]
(1)	(2)	(3)	(4)	(5)	(6)	(7)	(8)	(9)	(10)	(11)	(12)	(13)	(14)	(15)	(16)	(17)	(18)	(19)	(20)
1050	2.57714	34.2158	UGC 2105	SBab			2.0	53.2	4916	14.20	-20.58	3	0.2768	3	0.6822	3	5.0990	2	7.2750
1058	2.77972	34.7817	Mrk 1058	SBc			6.0	63.5	5109	15.34	-19.65	1	0.1398	2	0.1713	3	0.5870	2	1.3900
1066	2.94694	36.6217	UGC 2456	SBO-a			-0.3	53.1	3615	13.84	-20.25	3	0.4471	3	2.2630	2	10.9800	2	12.1500
1067	2.97856	42.3889	NGC 1164	SBab	R		1.7	40.9	4171	14.38	-20.25	3	0.1239	3	0.2012	2	1.9190	2	5.4000
1073	3.19525	41.8508	UGC 2608	SBb			3.0	21.5	7002	14.48	-21.24	3	0.4432	3	1.4120	2	8.1660	2	11.1100
1076	3.28581	0.3847	MCG 0- 9- 57	SBbc			4.3	64.0	7237	15.33	-20.23	1	0.0824	1	0.1870	3	0.3801	1	0.9465
1080	4.03217	-2.3239	NGC 1507	SBc		M	6.0	75.5	857	12.87	-18.17	1	0.1427	1	0.1391	2	1.6230	2	3.5280
1086	4.76603	-1.6253	MCG 0-13- 13	SBab			2.0	27.6	8995	14.83	-21.16	1	0.1182	2	0.1333	3	0.9421	2	1.2640
1088	4.86694	3.1886	NGC 1691	SBa	R		0.7	20.5	4595	12.76	-21.80	3	0.2659	3	0.8350	3	6.6050	2	10.7700
1092	5.03267	-10.1444	IC 401	SBbc			3.5	74.8	3286	14.50	-20.85	2	0.0997	2	0.0788	2	0.4782	1	3.6070
1118	17.82875	24.4947	NGC 6484	SBbc			3.7	13.5	3110	13.14	-20.58	3	0.1299	3	0.2085	3	1.6240	2	4.2260
1124	22.46953	-14.4447	NGC 7298	SBc			4.7	37.5	5035	14.29	-20.21	1	0.1058	1	0.0794	3	0.3817	2	1.5030
1149	0.89525	-14.5461	MCG -3- 3- 8	SB			...	60.3	6317	16.00	-18.70	1	0.1118	1	0.4020	3	0.5928	1	1.7040
1157	1.51081	35.4125	NGC 591	SBa			0.5	36.0	4550	14.15	-20.26	3	0.1549	3	0.4480	3	1.9910	2	3.4790
1171	1.97006	31.6411	NGC 783	SBc			5.2	31.3	5189	13.02	-21.65	3	0.1675	3	0.2884	3	2.0180	2	5.8520
1180	2.56344	33.1106	NGC 987	SBO-a			0.0	40.4	4487	13.54	-20.89	1	0.0908	1	0.0815	3	1.0870	2	3.1390
1194	5.15183	5.1406	NGC 1819	SBO			-2.0	52.9	4472	13.39	-21.26	3	0.2830	3	0.7071	2	6.6880	2	11.5000
1200	7.36553	27.4242	MCG 5-18- 11	SBab			2.0	...	7615	14.74	-20.83	1	0.2155	2	0.2799	2	1.3220	2	2.9990
1225	9.10994	15.9997	IC 528	SBab			2.0	62.0	3784	15.01	-19.03	1	0.0768	1	0.1413	3	0.2963	2	0.8287
1231	9.28525	-10.2903	MCG -2-24- 10	SB			...	53.0	11359	15.90	-20.00	1	0.0820	2	0.2003	3	1.1170	2	1.9910
1273	10.93783	-9.5769	MCG -2-28- 25	SBO-a			0.0	57.8	8184	15.29	-20.23	1	0.1240	1	0.1530	3	0.6890	2	1.2510
1291	11.35003	-8.3836	NGC 3660	SBb	R		3.0	36.8	3678	14.00	-20.68	2	0.1935	2	0.2236	3	1.8720	2	4.5360
1302	11.60581	3.8581	MCG 1-30- 5	SBb			3.0	52.2	5575	14.53	-22.90	1	0.0868	1	0.1966	3	0.5758	2	0.6442
1326	12.40389	8.1956	NGC 4416	SBc			5.4	27.2	1388	13.15	-18.44	2	0.1298	1	0.2220	3	0.9250	2	1.0330
1330	12.61792	-5.0700	NGC 4593	SBb		M	3.2	47.0	2496	11.80	-21.11	3	0.3441	2	0.8089	3	3.0520	2	5.9470
1341	12.97361	0.2414	NGC 4904	SBc			5.0	48.1	1171	12.62	-18.65	2	0.2220	2	0.3568	3	2.5550	2	7.1450
1344	13.11161	-5.0067	NGC 4990	SBO			-2.0	38.5	3172	14.50	-19.78	2	0.1780	3	0.5373	3	2.8170	2	2.5610
1346	13.31917	38.7997	NGC 5107	SBc			6.0	76.4	946	13.99	-17.61	1	0.0736	2	0.1249	3	0.8702	2	1.5340
1361	13.74347	11.3742	Mrk 1361	SB			...	...	6794	15.06	-19.30	2	0.1672	3	0.8386	3	3.2800	2	3.7340
1363	13.85617	-7.6853	NGC 5339	SBb			2.5	30.7	2663	16.50	-17.87	1	0.1896	1	0.3273	2	1.1070	2	3.1040
1365	13.86833	15.2892	UGC 8827	SBO			-2.0	39.5	5537	13.94	-20.74	2	0.1562	3	0.6445	3	4.2030	2	6.1130
1379	14.25050	-7.1869	NGC 5534	SBb		M	2.5	43.3	2630	13.04	-20.05	3	0.2524	3	0.8170	3	4.3570	2	6.2700
1433	10.51152	52.6294	UGC 5733	SBc			4.5	39.3	19037	15.05	-22.41	2	0.1039	2	0.0901	3	0.8773	2	1.7860
1452	11.68481	55.3250	MCG 9-19-165	SBc		M	5.5	38.9	6715	15.42	-19.74	1	0.0501	1	0.0712	3	0.3212	1	1.6530
1466	12.09372	3.1561	NGC 4123	SBc			4.5	42.3	1328	11.85	-19.65	2	0.3250	3	1.2360	3	6.2650	2	10.5200
1485	13.85406	40.6089	NGC 5350	SBbc			4.0	38.4	2303	12.22	-20.65	2	0.1411	3	0.3270	3	2.2200	2	8.7600

Table 3. Log of spectroscopic observations
(1) Markarian number
(2) Date of observation
(3) Exposure time (min)
(4) Spectral range (Å)
(5) Slit width (arcsec)
(6) Position angle of the slit (in degrees)

Mrk (1)	Date (2)	Exp. [min] (3)	Spec. range [Å] (4)	Width [arcsec] (5)	PA [°] (6)
4	04-03-93	30	3830-7360	2.7	76
10	06-03-93	30	3830-7360	2.7	305
12	05-03-93	30	3830-7360	2.7	356
13	07-03-93	45	3830-7360	2.7	0
21	13-01-94	45	3820-7375	2.7	90
31	06-03-93	30	3830-7360	2.7	0
38	15-03-92	45	3800-7310	3.1	57
39	22-12-93	45	3780-7335	2.7	70
42	14-01-94	45	3820-7375	2.7	142
52	01-02-93	45	4020-7365	2.4	90
58	14-01-94	45	3820-7375	2.7	142
78	07-03-93	45	3830-7360	2.7	281
79	14-03-92	30	3800-7310	3.1	239
86	01-02-93	45	4020-7365	2.4	90
87	14-03-92	30	3800-7310	3.1	48
90	02-01-92	30	3980-7310	2.2	357
114	01-01-92	25	3980-7310	2.2	145
122	01-01-92	25	3980-7310	2.2	115
133	02-01-92	20	3980-7310	2.2	300
141	02-04-91	45	3750-7674	2.8	104
152	06-03-93	30	3830-7360	2.7	330
161	02-01-92	20	3980-7310	2.2	255
179	14-03-92	20	3800-7310	3.1	90
185	02-03-93	38	3830-7360	2.7	0
188	15-03-92	20	3800-7310	3.1	121
213	02-04-91	40	3750-7674	2.8	144
271	03-03-93	45	3830-7360	2.7	74
291	06-03-93	50	3830-7360	2.7	355
300	04-03-93	40	3830-7360	2.7	0
306	17-09-91	60	3772-7714	2.8	188
307	18-09-91	60	3772-7714	2.8	7
323	02-01-92	25	3980-7310	2.2	207
332	18-09-91	45	3772-7714	2.8	103
353	17-09-91	60	3772-7714	2.8	34
373	07-03-93	45	3830-7360	2.7	0
374	21-12-93	30	3780-7335	2.7	113
382	07-03-93	45	3830-7360	2.7	0
384	01-02-93	45	4020-7365	2.4	0
401	01-01-92	20	3980-7310	2.2	161
412	22-12-93	45	3780-7335	2.7	165
446	15-03-92	30	3800-7310	3.1	342
471	05-03-93	30	3830-7360	2.7	40
474	06-03-93	30	3830-7360	2.7	355
479	05-03-93	30	3830-7360	2.7	22
489	05-03-93	30	3830-7360	2.7	0
493	05-03-93	30	3830-7360	2.7	48
534	02-01-92	20	3980-7310	2.2	207
545	17-09-91	60	3772-7714	2.8	158
571	02-01-92	15	3980-7310	2.2	261
575	01-01-92	40	3980-7310	2.2	228
593	21-12-93	23	3780-7335	2.7	180
602	01-01-92	20	3980-7310	2.2	33
617	13-01-94	40	3820-7375	2.7	194
618	07-03-93	45	3830-7360	2.7	0
620	01-01-92	20	3980-7310	2.2	114
665	14-03-92	30	3800-7310	3.1	334
691	02-04-91	60	3750-7674	2.8	94
708	01-02-93	45	4020-7365	2.4	90
710	01-01-92	30	3980-7310	2.2	213
712	13-01-94	45	3820-7375	2.7	188
718	14-01-94	45	3820-7375	2.7	142
731	01-01-92	20	3980-7310	2.2	342
752	21-12-93	30	3780-7335	2.7	18
759	02-01-92	20	3980-7310	2.2	255
766	14-01-94	30	3820-7375	2.7	142
781	04-03-93	30	3830-7360	2.7	8
803	06-03-93	30	3830-7360	2.7	355
804	15-03-92	30	3800-7310	3.1	154
814	02-03-93	45	3830-7360	2.7	0
860	03-03-93	30	3830-7360	2.7	52
874	05-03-93	30	3830-7360	2.7	302
1009	13-01-94	30	3820-7375	2.7	148
1026	02-01-92	30	3980-7310	2.2	315
1050	02-01-92	30	3980-7310	2.2	244
1058	14-01-94	45	3820-7375	2.7	270
1066	14-01-94	35	3820-7375	2.7	327
1067	21-12-93	30	3780-7335	2.7	146
1073	04-03-93	30	3830-7360	2.7	70
1076	21-12-93	45	3780-7335	2.7	148
1086	02-01-92	40	3980-7310	2.2	315
1088	01-01-92	20	3980-7310	2.2	25
1171	13-01-94	25	3820-7375	2.7	92
1180	14-01-94	30	3820-7375	2.7	216
1194	14-03-92	30	3800-7310	3.1	311
1200	15-03-92	30	3800-7310	3.1	312
1231	21-12-93	45	3780-7335	2.7	13
1273	21-12-93	45	3780-7335	2.7	42
1291	04-03-93	45	3830-7365	2.7	325
1302	21-12-93	45	3780-7335	2.7	32
1326	13-01-94	45	3820-7375	2.7	188
1330	04-03-93	30	3830-7360	2.7	56
1341	01-01-92	20	3980-7310	2.2	317
1346	15-03-92	30	3800-7310	3.1	122
1361	14-01-94	40	3820-7375	2.7	142
1363	14-03-92	60	3800-7310	3.1	90
1365	04-03-93	30	3830-7360	2.7	80
1379	15-03-92	30	3800-7310	3.1	88
1433	02-01-92	25	3980-7310	2.2	300
1452	13-01-94	45	3820-7375	2.7	188
1466	15-03-92	30	3800-7310	3.1	105
1485	02-03-93	45	3830-7360	2.7	24

Table 4. Measured spectrophotometric data. Observed intensities and equivalent widths of emission lines.

(1) Markarian number

(2) Number of the emission-line region in the galaxy

(3) Position: nuclear (= 1) or extranuclear (= 0) emission-line region

(4) Distance between extranuclear emission-line regions and the galaxy nucleus (in arcsec)

(5) Size of emission-line regions (in arcsec)

(6-21) Observed intensity F_λ ($\times\ 10^{-14}$ erg cm^{-2}s^{-1}) and equivalent width W_λ (Å) of emission lines:

- (6-7) H$\beta\lambda$4861,
- (8-9) [O III]λ4959,
- (10-11) [O III]λ5007,
- (12-13) [N II]λ6548,
- (14-15) H$\alpha\lambda$6563,
- (16-17) [N II]λ6583,
- (18-19) [S II]λ6716,
- (20-21) [S II]λ6731

Mrk	H II				Hβλ4861		[O III]λ4959		[O III]λ5007		[N II]λ6548		Hαλ6563		[N II]λ6583		[S II]λ6716		[S II]λ6731	
	num	pos	dist	size	F_λ	W_λ	F_λ	W_λ	F_λ	W_λ	F_λ	W_λ	F_λ	W_λ	F_λ	W_λ	F_λ	W_λ	F_λ	W_λ
(1)	(2)	(3)	(4)	(5)	(6)	(7)	(8)	(9)	(10)	(11)	(12)	(13)	(14)	(15)	(16)	(17)	(18)	(19)	(20)	(21)
4	...	1	...	6.9	<1.10	...	...	...	...	...	0.12	-3.07	3.14	-80.68	0.22	-5.82	0.32	-9.32	0.44	-12.61
10	1	1	...	2.3	14.26	-48.92	3.83	-13.49	12.49	-45.82	...	...	...	...	...	...	...	...	...	...
	2	0	14.9	8.0	<0.40	...	...	...	...	...	0.17	-2.79	1.13	-17.98	0.31	-4.95	...	...	...	...
	3	0	43.7	3.4	<0.19	...	...	...	...	...	0.03	-6.15	0.54	-107.68	0.05	-10.77	...	...	...	...
12	1	0	21.8	8.0	0.39	-8.80	...	...	0.67	-18.66	...	...	1.47	-50.60	0.31	-10.72	0.25	-9.04	0.20	-7.32
	2	0	12.6	5.8	0.71	-10.72	0.62	-10.55	0.78	-14.12	0.11	-2.52	2.34	-49.37	0.52	-11.49	0.32	-6.71	0.26	-5.59
	3	0	6.9	3.4	0.37	-5.25	...	...	...	...	0.10	-1.97	1.96	-38.30	0.60	-12.21	0.15	-3.18	0.43	-8.98
	4	1	...	8.0	2.21	-8.55	...	...	0.57	-2.37	0.76	-4.27	11.61	-62.40	3.09	-17.20	1.94	-10.87	1.14	-6.49
	5	0	8.0	4.6	0.48	-7.66	...	...	...	...	0.22	-5.16	2.00	-47.42	0.79	-18.48	0.23	-5.53	0.48	-11.69
	6	0	14.9	6.9	0.27	-3.78	...	...	0.52	-7.25	0.12	-2.41	1.69	-33.63	0.36	-7.24	...	...	...	...
13	1	1	...	3.4	1.62	-38.13	0.79	-18.50	2.82	-68.08	0.22	-7.24	5.50	-170.92	0.72	-24.15	0.48	-15.05	0.39	-12.35
	2	0	4.6	3.4	1.47	-27.42	0.71	-13.87	2.14	-41.71	0.16	-4.30	7.34	-191.83	0.76	-20.27	0.81	-20.58	0.52	-13.65
21	1	0	16.1	6.9	<0.08	...	...	...	...	...	0.01	-1.20	0.23	-19.48	0.07	-5.93	...	...	...	...
	2	1	...	2.3	0.15	-1.69	0.12	-1.32	0.08	-0.89	0.09	-1.03	2.24	-26.04	0.68	-7.92	...	...	...	...
	3	0	3.4	2.3	<0.69	...	...	...	...	...	0.11	-0.64	1.97	-11.07	0.87	-4.98	...	...	...	...
	4	0	18.4	9.2	<0.15	...	...	...	...	...	0.05	-2.80	0.44	-25.60	0.31	-18.01	...	...	...	...
31	1	0	19.5	9.2	<0.21	...	...	...	...	...	...	...	0.59	-37.96	0.15	-9.71	...	...	...	...
	2	1	...	3.4	0.67	-8.03	...	...	0.24	-2.83	0.14	-2.00	3.70	-51.73	1.07	-14.92	0.60	-9.63	0.44	-7.16
	3	0	10.3	3.4	<0.16	...	...	...	...	...	...	...	0.45	-34.83	0.08	-6.09	...	...	...	...
38	...	1	...	6.9	0.21	-2.47	0.04	-0.51	0.49	-5.65	0.11	-1.51	2.44	-34.57	0.82	-11.61	0.40	-5.93	0.37	-5.46
39	1	1	...	6.9	0.26	-3.68	0.18	-2.61	0.54	-8.06	0.02	-0.54	1.53	-35.98	0.23	-5.37	0.30	-7.23	0.20	-4.76
	2	0	8.0	5.8	0.05	-2.43	0.08	-4.42	0.12	-6.33	0.01	-0.65	0.42	-39.83	0.08	-7.51	0.09	-8.78	0.06	-5.96
42	1	0	9.2	2.3	0.07	-5.19	0.01	-0.83	0.06	-4.50	...	...	0.53	-37.06	0.14	-1.50	0.04	-3.24	0.07	-5.43
	2	1	...	2.3	3.23	-28.89	0.21	-1.92	2.05	-19.02	2.27	-19.24	10.75	-91.62	4.28	-35.97	0.20	-1.87	0.13	-1.25
52	...	1	...	4.6	26.85	-38.25	6.05	-8.95	17.65	-26.56	12.91	-30.67	77.19	-184.18	36.77	-88.10	7.06	-17.54	6.74	-16.77
58	...	1	...	6.9	<0.50	...	...	...	...	...	0.08	-1.17	1.42	-21.54	0.52	-7.87	0.22	-3.33	0.25	-3.68
78	...	1	...	5.7	3.75	-17.25	16.23	-72.92	49.08	-225.57	2.24	-9.40	21.92	-92.61	19.04	-79.81	6.18	-26.12	4.79	-19.86
86	1	0	32.2	10.3	0.48	-2.16	0.49	-2.23	3.53	-16.25	...	...	3.08	-22.91	0.35	-2.64	...	...	...	...
	2	1	...	6.9	11.42	-30.97	8.26	-23.35	23.51	-67.45	0.12	-0.53	37.36	-160.11	5.32	-23.08	4.80	-21.61	3.41	-15.40
87	...	1	...	6.9	<1.60	...	...	...	...	...	0.27	-1.27	4.55	-21.17	1.80	-8.47	0.69	-3.35	0.56	-2.74
90	1	0	7.0	11.0	0.41	-3.45	...	...	...	...	0.33	-2.63	3.12	-24.82	1.19	-9.58	0.23	-1.78	0.26	-2.04
	2	1	...	4.0	0.24	-2.53	...	...	...	...	0.45	-4.11	2.94	-27.59	2.51	-23.06	0.34	-3.22	0.35	-3.33
	3	0	10.0	8.0	<0.34	...	...	...	...	...	0.18	-2.97	0.96	-15.70	0.41	-6.71	...	...	...	...
114	...	1	...	6.0	<2.30	...	...	...	...	...	0.99	-3.83	6.56	-25.33	3.27	-12.64	0.22	-0.87	0.23	-0.90
122	1	0	9.0	4.0	0.37	-11.21	...	...	...	...	0.19	-6.23	1.37	-46.57	0.59	-20.14	...	...	...	...
	2	1	...	3.0	<1.80	...	...	...	...	...	0.93	-3.82	5.14	-21.11	2.71	-11.21	...	...	...	...
	3	0	10.0	4.0	<0.47	...	...	...	...	...	0.17	-4.69	1.35	-39.47	0.33	-9.49	...	...	...	...
133	1	0	8.0	5.0	<0.30	...	...	...	...	...	0.09	-1.65	0.87	-16.47	0.29	-5.51	...	...	...	...
	2	1	...	4.0	2.52	-9.56	0.36	-1.38	0.48	-1.87	1.41	-5.76	14.02	-56.29	5.75	-23.46	1.47	-6.01	1.48	-6.14
	3	0	9.0	8.0	0.46	-4.36	...	...	...	...	0.31	-2.97	2.36	-22.81	0.76	-7.44	0.42	-4.07	0.29	-2.75
	4	0	20.0	5.0	<0.19	...	...	...	...	...	...	...	0.55	-28.82	0.19	-9.90	...	...	...	...
152	1	1	...	2.3	0.47	-4.82	...	...	...	...	0.24	-3.50	2.46	-36.33	1.22	-18.10	...	...	...	...
	2	0	8.0	5.8	<0.28	...	...	...	...	...	0.25	-3.88	0.80	-12.63	0.84	-12.95	...	...	...	...

Mrk	H II				Hβλ4861		[O III]λ4959		[O III]λ5007		[N II]λ6548		Hαλ6563		[N II]λ6583		[S II]λ6716		[S II]λ6731	
	num	pos	dist	size	F_λ	W_λ	F_λ	W_λ	F_λ	W_λ	F_λ	W_λ	F_λ	W_λ	F_λ	W_λ	F_λ	W_λ	F_λ	W_λ
(1)	(2)	(3)	(4)	(5)	(6)	(7)	(8)	(9)	(10)	(11)	(12)	(13)	(14)	(15)	(16)	(17)	(18)	(19)	(20)	(21)
161	1	0	12.0	4.0	0.65	-10.16	0.39	-6.65	0.77	-13.30	0.46	-9.23	4.12	-88.11	1.49	-32.25	0.58	-12.83	0.34	-7.72
	2	1	...	2.0	0.61	-3.73	0.56	-3.46	0.87	-5.29	1.38	-9.44	6.20	-42.89	3.58	-24.96	0.77	-5.27	0.38	-2.61
	3	0	11.0	4.0	1.13	-14.79	0.41	-5.62	0.81	-10.89	0.85	-14.31	5.92	-108.16	2.22	-40.22	0.80	-14.21	0.37	-6.58
179	1	1	...	6.9	0.25	-7.45	0.11	-3.42	...	...	0.03	-0.91	0.86	-31.60	0.23	-7.81	0.20	-7.20	0.06	-1.97
	2	0	14.9	3.4	<0.13	...	...	...	...	...	0.07	-0.64	0.37	-3.28	0.29	-2.55	...	...	...	...
	3	0	34.5	5.8	<0.30	...	...	...	...	...	0.14	-5.82	0.81	-32.97	0.67	-26.96	...	...	...	...
185	1	0	16.1	10.3	0.11	-1.63	...	...	...	...	0.01	-0.21	0.89	-15.49	0.22	-3.93	...	...	...	...
	2	1	...	5.8	<1.06	...	...	...	...	...	0.31	-1.36	3.02	-13.37	1.27	-5.63	0.34	-1.53	0.27	-1.20
	3	0	23.0	11.5	0.18	-3.55	...	...	...	...	...	...	1.26	-32.41	0.40	-10.13	0.20	-5.07	0.13	-3.24
	4	0	33.3	5.8	0.15	-11.71	...	...	...	...	0.05	-4.49	1.06	-101.32	0.20	-19.56	0.11	-10.52	0.12	-11.74
188	1	0	17.2	8.0	0.79	-7.69	...	...	0.12	-1.30	0.10	-1.18	5.43	-63.59	1.17	-13.58	...	...	...	...
	2	1	...	4.6	0.35	-1.49	...	...	0.12	-0.53	0.15	-0.61	4.49	-18.03	1.09	-4.39	0.52	-2.23	0.21	-0.91
	3	0	11.5	4.6	0.45	-4.32	...	...	0.06	-0.61	0.20	-2.27	4.30	-48.24	1.11	-12.23	0.35	-3.97	0.41	-4.64
213	1	0	18.2	5.2	2.72	-16.41	1.34	-8.79	2.96	-20.36	1.68	-13.86	12.67	-108.33	3.06	-25.51	1.15	-9.93	1.10	-9.39
	2	1	...	5.2	18.35	-9.44	14.61	-7.64	43.15	-23.64	8.30	-4.81	107.82	-61.93	51.78	-29.58	11.40	-6.38	9.43	-5.25
271	1	1	...	11.5	0.18	-0.85	0.77	-3.74	0.73	-3.55	0.66	-3.33	2.83	-14.27	1.96	-9.92	...	...	...	...
	2	0	13.8	8.0	<0.38	...	0.13	-1.52	0.21	-2.43	0.24	-3.64	1.08	-16.44	0.59	-8.93	...	...	...	...
	3	1	...	8.0	0.06	-0.47	0.89	-6.24	2.37	-16.61	0.54	-4.39	1.49	-12.09	1.28	-10.33	...	...	...	...
300	...	1	...	4.6	0.18	-0.82	0.32	-1.51	0.30	-1.44	0.69	-3.46	4.88	-24.48	2.89	-14.46	0.68	-3.44	0.69	-3.46
306	1	0	9.1	5.2	0.57	-11.04	0.39	-8.14	1.02	-21.64	...	...	2.28	-78.02	0.45	-15.02	0.35	-12.70	0.34	-12.55
	2	1	...	3.9	0.70	-10.84	0.22	-3.57	0.65	-10.70	0.20	-5.14	2.90	-74.38	0.99	-25.61	0.48	-13.33	0.51	-14.17
	3	0	5.2	2.6	0.56	-10.68	0.22	-4.11	0.65	-12.89	0.18	-5.32	2.78	-80.92	0.77	-22.57	0.42	-12.75	0.33	-10.27
	4	0	7.8	9.1	1.30	-11.37	0.45	-3.73	1.49	-12.93	0.42	-5.34	5.77	-75.94	1.49	-19.24	0.88	-11.44	0.66	-8.67
307	1	0	11.7	2.6	0.18	-9.06	0.10	-5.10	0.15	-7.68	...	...	0.56	-37.15	0.19	-12.74	0.12	-8.70	0.09	-6.54
	2	0	6.5	3.9	0.30	-5.51	0.05	-0.94	0.26	-4.69	0.29	-7.49	2.00	-51.33	0.82	-21.31	0.58	-15.16	0.19	-4.91
	3	1	...	3.9	0.59	-3.02	0.25	-1.25	0.24	-1.22	0.57	-3.83	4.25	-28.73	1.60	-10.80	0.55	-3.66	0.56	-3.77
	4	0	5.2	3.9	0.09	-4.13	...	...	...	...	0.07	-4.78	0.58	-36.41	0.24	-15.74	0.10	-6.16	0.09	-5.56
	5	0	10.4	3.9	0.40	-10.75	0.11	-2.92	0.40	-10.87	0.09	-3.19	1.79	-63.41	0.55	-19.53	0.16	-5.86	0.40	-14.21
323	1	0	13.0	10.0	0.57	-9.01	...	...	...	...	0.41	-6.52	2.56	-39.75	0.91	-14.44	0.36	-5.81	0.30	-4.76
	2	0	3.0	2.0	0.43	-10.97	...	...	...	...	0.20	-5.15	2.66	-67.15	0.66	-16.57	0.19	-4.45	...	...
	3	1	...	9.0	1.44	-7.96	...	...	...	...	0.70	-3.34	8.84	-41.70	2.68	-12.67	0.63	-2.93	0.36	-1.65
	4	0	14.0	7.0	0.27	-4.29	...	...	...	...	0.15	-2.45	1.68	-26.61	0.58	-9.09	...	...	...	...
332	1	0	10.4	6.5	0.67	-9.15	0.10	-1.46	0.19	-2.77	0.10	-1.95	3.74	-70.36	0.95	-18.08	0.57	-10.49	0.23	-4.23
	2	1	...	2.6	0.66	-1.83	0.55	-1.54	0.23	-0.64	1.82	-5.74	6.75	-21.19	5.31	-16.66	1.65	-5.22	1.43	-4.52
	3	0	9.1	7.8	0.59	-4.17	0.29	-2.17	0.20	-1.50	0.14	-1.24	4.66	-39.51	1.31	-11.18	0.62	-5.35	0.40	-3.42
	4	0	23.4	6.5	0.32	-5.94	...	...	0.35	-6.56	0.39	-8.80	1.46	-32.85	0.96	-21.63	...	...	...	...
353	...	1	...	6.5	1.16	-4.80	0.66	-2.68	1.88	-7.74	2.22	-8.99	11.57	-46.81	8.11	-32.76	1.81	-7.06	1.50	-5.84
373	...	1	...	4.6	1.51	-9.50	0.67	-4.23	1.54	-9.85	1.71	-11.90	10.82	-75.00	5.22	-36.22	1.49	-10.21	1.44	-9.88
384	1	0	10.3	4.6	0.10	-5.45	...	...	...	...	0.13	-4.54	0.67	-24.17	0.34	-12.31	0.14	-4.75	0.07	-2.26
	2	1	...	3.4	0.65	-2.47	...	...	...	...	1.23	-5.22	6.84	-29.43	3.61	-15.38	0.60	-2.57	0.70	-2.98
401	1	0	10.0	7.0	0.42	-7.40	...	...	...	...	0.31	-5.32	1.63	-30.29	0.73	-13.71	0.18	-3.44	0.27	-5.13
	2	1	...	4.0	3.82	-6.47	0.62	-1.03	1.14	-1.95	3.34	-7.33	22.30	-50.48	11.67	-25.68	2.36	-5.27	2.63	-5.94
412	...	1	...	5.7	4.40	-24.05	4.90	-27.17	15.28	-87.10	...	...	17.40	-155.84	1.48	-13.18	1.75	-15.47	1.26	-11.22

Mrk	H II				Hβλ4861		[O III]λ4959		[O III]λ5007		[N II]λ6548		Hαλ6563		[N II]λ6583		[S II]λ6716		[S II]λ6731	
	num	pos	dist	size	F_λ	W_λ	F_λ	W_λ	F_λ	W_λ	F_λ	W_λ	F_λ	W_λ	F_λ	W_λ	F_λ	W_λ	F_λ	W_λ
(1)	(2)	(3)	(4)	(5)	(6)	(7)	(8)	(9)	(10)	(11)	(12)	(13)	(14)	(15)	(16)	(17)	(18)	(19)	(20)	(21)
446	1	0	17.2	4.6	0.26	-10.10	0.26	-11.19	...	...	0.05	-2.42	1.31	-64.48	0.39	-19.30	...	...	...	...
	2	1	...	4.6	0.35	-0.87	0.60	-1.49	0.21	-0.54	0.31	-0.89	7.36	-21.39	3.22	-9.35	...	...	...	...
	3	0	20.7	5.8	<0.28	...	...	...	...	...	0.03	-2.49	0.81	-61.05	0.21	-16.46	...	...	...	...
471	...	1	...	5.7	<0.63	...	0.98	-4.28	2.09	-9.33	0.98	-4.46	1.79	-8.14	2.13	-9.70	0.44	-2.16	0.36	-1.79
479	1	1	...	4.6	1.44	-11.21	...	...	...	...	0.29	-3.09	8.04	-87.23	1.43	-15.29	0.98	-10.68	0.51	-5.80
	2	0	18.4	4.6	1.09	-16.62	0.55	-8.45	1.79	-27.75	...	...	4.51	-102.15	0.79	-18.22	0.54	-12.23	0.48	-10.75
489	1	0	9.2	6.9	<0.47	...	...	...	0.51	-7.24	0.08	-1.77	1.33	-28.33	0.44	-9.76	0.17	-3.87	0.19	-4.35
	2	1	...	5.8	1.66	-4.94	1.28	-3.83	2.03	-6.11	0.54	-2.41	12.51	-56.25	3.24	-14.46	1.94	-9.00	1.21	-5.58
	3	0	8.0	3.4	<0.43	...	0.09	-2.10	0.31	-7.13	0.04	-1.21	1.24	-37.05	0.24	-7.52	0.23	-6.87	0.20	-6.04
534	1	1	...	6.0	5.29	-5.16	2.70	-2.65	8.77	-8.78	6.40	-8.07	44.97	-56.62	18.57	-23.32	4.77	-6.02	3.59	-4.56
	2	0	9.0	3.0	0.59	-17.05	0.53	-17.62	0.90	-29.99	0.32	-8.28	3.73	-100.58	0.98	-26.59	0.57	-15.85	0.30	-8.33
545	1	1	...	6.5	4.11	-3.12	1.97	-1.51	2.87	-2.27	8.68	-8.02	30.48	-28.34	22.53	-20.74	6.88	-6.49	4.59	-4.25
	2	0	19.5	3.9	0.87	-14.46	0.20	-3.38	0.42	-7.20	0.66	-13.76	4.20	-91.19	2.11	-46.21	0.56	-12.35	0.40	-8.60
571	...	1	...	4.0	0.70	-3.59	...	...	...	...	0.78	-3.60	6.70	-31.01	3.13	-14.50	0.79	-3.70	0.46	-2.15
575	1	0	12.0	5.0	0.56	-16.66	...	...	...	...	0.27	-7.14	2.25	-58.48	0.66	-17.29	0.31	-8.15	0.17	-4.53
	2	1	...	2.0	0.99	-5.48	...	...	...	...	1.21	-6.93	7.17	-41.21	3.62	-20.73	0.73	-4.20	0.62	-3.59
593	...	1	...	5.7	<0.66	...	...	...	...	...	0.57	-2.28	1.87	-7.46	1.05	-4.16	...	...	...	...
602	...	1	...	4.0	1.77	-7.66	0.52	-2.25	0.75	-3.28	2.36	-9.07	17.24	-66.63	7.01	-27.20	2.41	-9.31	2.02	-7.73
617	...	1	...	4.6	2.65	-10.78	0.76	-3.05	2.85	-11.36	5.96	-20.34	29.16	-99.40	21.29	-72.08	3.53	-11.55	3.76	-12.22
618	1	1	...	3.4	5.63	-40.61	1.06	-7.28	3.66	-26.46	...	...	...	...	...	...	...	...	...	...
	2	0	11.5	5.8	<0.47	...	...	...	...	...	...	...	1.34	-36.45	0.43	-11.54	0.09	-2.50	0.15	-3.99
620	...	1	...	4.0	2.06	-3.88	7.66	-14.26	21.30	-40.49	5.41	-8.70	23.29	-37.26	18.67	-30.06	4.48	-7.27	5.50	-8.94
665	1	1	...	2.3	0.22	-1.59	0.49	-3.36	0.66	-4.51	0.36	-2.19	2.96	-18.03	1.48	-8.97	0.27	-1.79	0.33	-2.23
	2	0	9.2	5.8	0.13	-2.55	0.16	-3.05	0.09	-1.74	0.03	-0.67	1.10	-21.75	0.27	-5.22	0.11	-2.34	0.08	-1.74
691	1	0	11.7	7.8	5.27	-25.90	3.06	-15.95	9.45	-49.76	...	...	24.28	-164.36	2.13	-15.03	2.94	-21.59	2.34	-16.70
	2	1	...	6.5	12.25	-16.08	1.30	-1.81	3.48	-5.00	...	...	69.89	-125.88	15.15	-27.67	6.11	-11.08	6.48	-11.67
708	...	1	...	5.7	3.30	-8.05	0.55	-1.33	0.93	-2.23	4.64	-10.51	25.76	-58.01	11.79	-26.48	4.75	-10.67	3.65	-8.21
710	1	0	11.0	10.0	1.87	-12.42	0.26	-1.77	0.56	-3.91	0.83	-6.29	10.35	-78.02	2.75	-21.02	1.56	-12.22	1.11	-8.77
	2	0	3.0	3.0	3.88	-27.44	0.45	-3.28	1.32	-9.94	1.27	-12.54	15.27	-152.66	5.17	-51.48	1.68	-16.85	1.43	-14.10
	3	1	...	4.0	5.81	-35.96	0.47	-3.13	1.98	-13.45	2.18	-19.67	22.56	-205.31	8.44	-76.39	2.75	-25.47	2.13	-19.42
712	1	0	5.8	4.6	2.66	-53.85	2.68	-56.09	8.09	-169.97	0.47	-13.49	9.49	-272.26	1.24	-35.11	0.54	-15.02	0.39	-10.53
	2	1	...	2.3	0.42	-9.48	0.37	-8.55	1.06	-24.82	0.04	-1.25	1.73	-54.87	0.41	-13.14	0.26	-8.00	0.15	-4.65
	3	0	8.0	8.0	0.38	-10.13	0.13	-3.38	0.50	-13.15	0.02	-0.66	0.84	-33.08	0.33	-13.12	0.21	-8.55	0.16	-6.44
718	1	0	8.0	2.3	0.05	-2.06	...	...	...	...	...	-0.12	0.89	-28.32	0.24	-7.65	0.08	-2.61	0.07	-2.30
	2	1	...	3.4	0.13	-0.90	...	...	0.08	-0.52	0.18	-0.97	2.66	-14.10	1.16	-6.15	0.16	-0.84	0.12	-0.65
	3	0	11.5	2.3	0.10	-4.53	0.01	-0.68	0.03	-1.30	0.03	-1.52	0.86	-44.34	0.30	-15.76	0.08	-4.43	0.04	-2.03
731	1	0	4.0	3.0	<1.52	...	0.21	-1.30	0.19	-1.17	0.63	-3.79	4.34	-25.87	1.94	-11.61	0.75	-4.51	0.74	-4.39
	2	1	...	3.0	1.85	-11.06	0.21	-1.26	0.33	-1.97	2.27	-14.72	16.38	-104.79	7.59	-48.41	2.13	-13.70	2.01	-12.84
752	1	1	...	9.2	0.45	-6.48	0.29	-4.32	0.49	-7.37	0.06	-1.24	2.49	-49.64	0.62	-12.40	0.27	-5.44	0.13	-2.59
	2	0	10.3	8.0	0.29	-5.06	0.21	-3.84	0.60	-11.15	...	...	1.63	-44.41	0.35	-9.37	0.19	-5.36	0.08	-2.26
759	...	1	...	5.0	0.65	-3.44	...	...	...	...	0.93	-4.57	5.41	-26.82	2.66	-13.24	0.41	-2.02	0.44	-2.15
781	1	0	25.3	13.8	0.37	-4.09	...	...	0.41	-4.54	0.02	-0.23	2.22	-32.13	0.69	-10.01	0.35	-5.38	...	...
	2	1	...	5.8	2.14	-6.64	...	...	0.29	-0.95	0.90	-3.50	12.40	-48.00	4.44	-17.16	1.49	-5.87	1.08	-4.22
	3	0	23.0	5.8	<0.58	...	...	...	...	...	...	...	1.66	-37.66	0.38	-8.41	0.26	-5.72	0.17	-3.86
	4	0	32.2	9.2	0.20	-3.95	0.11	-2.45	0.42	-8.57	0.03	-0.87	1.38	-37.59	0.34	-9.13	0.13	-3.91	0.29	-8.52

Mrk	H II				Hβλ4861		[O III]λ4959		[O III]λ5007		[N II]λ6548		Hαλ6563		[N II]λ6583		[S II]λ6716		[S II]λ6731	
	num	pos	dist	size	F_λ	W_λ	F_λ	W_λ	F_λ	W_λ	F_λ	W_λ	F_λ	W_λ	F_λ	W_λ	F_λ	W_λ	F_λ	W_λ
(1)	(2)	(3)	(4)	(5)	(6)	(7)	(8)	(9)	(10)	(11)	(12)	(13)	(14)	(15)	(16)	(17)	(18)	(19)	(20)	(21)
803	...	1	...	5.7	3.92	-17.72	5.07	-23.76	15.51	-74.29	0.45	-3.46	13.37	-102.42	1.16	-8.88	1.33	-10.41	0.80	-6.25
804	1	0	6.9	9.2	0.23	-6.12	0.16	-4.62	0.21	-5.77	0.03	-1.02	1.32	-49.17	0.34	-12.70	0.18	-7.18	0.16	-6.58
	2	1	...	6.9	0.40	-5.55	0.17	-2.50	1.61	-23.22	0.17	-2.98	2.22	-39.08	1.11	-19.58	0.36	-6.50	0.32	-5.74
	3	0	6.9	11.5	0.16	-5.00	0.07	-2.39	0.25	-8.38	...	...	1.15	-45.57	0.27	-10.73	0.20	-8.31	0.15	-6.29
814	1	0	23.0	5.8	0.04	-2.55	0.04	-2.39	0.08	-5.60	0.01	-0.92	0.49	-44.29	0.16	-14.63	0.11	-10.19	0.10	-9.02
	2	0	11.5	6.9	0.07	-1.33	0.26	-5.16	0.19	-3.74	0.10	-2.34	1.08	-25.02	0.38	-8.67	0.19	-4.55	0.15	-3.63
	3	1	...	4.6	0.34	-1.72	0.15	-0.77	0.14	-0.69	0.75	-3.52	4.37	-20.47	2.47	-11.56	0.85	-4.02	0.67	-3.12
	4	0	10.3	5.8	<0.14	...	...	...	...	...	0.03	-0.55	0.41	-8.12	0.24	-4.65	0.09	-1.76	0.08	-1.67
	5	0	24.1	5.8	<0.09	...	0.03	-1.63	0.11	-6.59	...	...	0.27	-20.82	0.09	-6.59	...	...	...	...
	6	0	43.7	2.3	<0.04	...	...	...	...	...	...	...	0.11	-57.60	0.01	-7.02	...	...	...	...
860	1	1	...	5.8	0.48	-14.14	0.66	-19.61	1.89	-56.49	0.09	-3.39	2.13	-78.84	0.57	-21.12	0.13	-5.05	0.29	-11.10
	2	0	4.6	5.8	0.61	-16.80	0.74	-20.76	2.11	-59.74	0.18	-6.15	2.36	-80.04	0.79	-26.61	0.29	-9.85	0.27	-9.34
	3	0	4.6	4.6	0.48	-9.72	0.16	-3.45	0.18	-3.92	0.19	-5.02	2.60	-67.24	1.08	-27.95	0.08	-2.05	0.21	-5.29
	4	1	...	4.6	0.53	-9.60	0.13	-2.52	0.33	-6.33	0.62	-13.75	2.88	-63.45	1.81	-40.08	0.16	-3.62	0.32	-7.23
874	1	1	...	5.8	0.67	-6.84	0.61	-6.52	1.92	-20.85	0.05	-0.93	3.19	-57.03	0.39	-7.16	0.72	-13.43	0.48	-8.83
	2	0	4.6	3.4	1.31	-20.66	1.17	-19.45	3.54	-61.06	0.06	-1.60	4.49	-132.24	0.43	-12.95	0.54	-16.46	0.38	-11.89
	3	1	...	3.4	1.48	-26.33	1.13	-20.88	3.31	-63.21	0.10	-3.07	5.52	-167.55	0.70	-21.06	0.79	-24.99	0.57	-17.96
1009	1	0	20.7	6.9	0.31	-6.51	0.14	-2.91	0.48	-10.14	0.08	-2.10	1.89	-46.74	0.60	-15.30	0.37	-9.01	0.19	-4.87
	2	1	...	4.6	0.86	-2.78	0.69	-2.22	0.39	-1.28	0.34	-1.08	7.20	-22.34	2.63	-8.19	1.14	-3.55	0.86	-2.68
	3	0	17.2	8.0	0.15	-1.71	0.17	-1.98	0.12	-1.47	0.07	-0.92	1.71	-23.33	0.71	-9.60	0.37	-4.87	0.19	-2.47
1026	1	0	22.0	7.0	<0.42	...	...	...	...	...	...	...	1.20	-62.68	0.13	-7.38	0.27	-15.42	0.03	-1.62
	2	1	...	5.0	0.33	-2.28	0.41	-2.77	0.33	-2.20	0.38	-2.27	4.73	-27.78	1.90	-11.48	0.86	-5.20	0.48	-2.88
1050	...	1	...	5.0	1.27	-5.02	...	...	...	...	2.14	-8.14	12.64	-48.14	6.80	-25.49	1.24	-4.72	1.57	-6.00
1058	...	1	...	6.9	0.34	-1.46	2.83	-11.89	8.67	-36.59	0.64	-2.20	6.45	-22.09	4.06	-13.84	1.28	-4.30	1.65	-5.48
1066	...	1	...	5.7	7.07	-15.40	9.55	-20.25	29.14	-61.52	16.06	-26.49	56.62	-91.88	51.27	-83.86	12.00	-18.64	12.66	-19.69
1067	...	1	...	5.7	<1.94	...	...	...	...	...	0.79	-1.27	5.54	-8.96	3.33	-5.37	0.67	-1.08	0.54	-0.87
1073	1	0	10.3	9.2	1.22	-10.35	...	...	1.84	-15.60	0.47	-4.31	7.70	-69.51	2.26	-20.50	0.59	-5.64	0.31	-2.99
	2	1	...	4.6	4.77	-21.65	11.83	-53.07	32.26	-145.73	7.76	-33.51	23.07	-101.85	21.75	-92.96	4.09	-17.67	3.31	-14.23
	3	0	11.5	3.4	<1.11	...	0.40	-7.40	0.75	-13.40	0.78	-14.96	3.17	-62.43	1.78	-34.26	...	...	...	...
1076	...	1	...	6.9	0.78	-6.84	0.23	-2.01	0.33	-2.96	0.25	-2.71	5.78	-62.98	1.62	-17.66	0.36	-4.05	0.40	-4.44
1086	1	0	7.0	5.0	<0.21	...	...	...	...	...	0.12	-4.69	0.61	-22.62	0.29	-11.29	...	...	...	...
	2	1	...	4.0	0.48	-4.20	...	...	...	...	1.05	-9.25	4.59	-40.44	2.48	-21.60	0.73	-7.05	0.55	-5.22
	3	0	5.0	4.0	0.49	-9.54	0.49	-9.54	...	...	0.23	-5.89	1.07	-26.79	0.44	-11.00	0.67	-16.18	0.65	-15.72
1088	...	1	...	6.0	2.80	-2.90	1.15	-1.20	0.58	-0.62	6.41	-6.55	28.27	-28.77	17.16	-17.50	3.98	-4.07	3.63	-3.70
1171	1	0	24.1	6.9	0.34	-3.42	...	...	0.09	-1.00	0.10	-0.94	1.51	-13.91	0.61	-5.73	0.17	-1.68	0.26	-2.59
	2	1	...	6.9	0.52	-1.58	...	...	...	...	0.38	-1.37	7.75	-27.33	2.78	-9.88	0.58	-2.05	0.56	-1.97
	3	0	20.7	4.6	0.08	-1.92	...	...	...	...	0.02	-0.66	0.96	-29.88	0.33	-10.27	0.09	-2.62	0.07	-2.19
1180	...	1	...	5.7	<0.77	...	...	...	...	...	0.43	-0.57	2.19	-2.89	2.31	-3.04	0.13	-0.17	0.33	-0.43
1194	...	1	...	9.2	1.11	-1.78	...	...	...	...	1.50	-2.51	17.93	-30.10	7.85	-13.24	1.58	-2.75	0.84	-1.45
1200	...	1	...	5.7	<1.05	...	0.53	-2.20	1.10	-4.55	1.13	-4.43	3.00	-11.72	2.18	-8.52	...	...	...	...

Mrk	H II				Hβλ4861		[O III]λ4959		[O III]λ5007		[N II]λ6548		Hαλ6563		[N II]λ6583		[S II]λ6716		[S II]λ6731	
	num	pos	dist	size	F_λ	W_λ	F_λ	W_λ	F_λ	W_λ	F_λ	W_λ	F_λ	W_λ	F_λ	W_λ	F_λ	W_λ	F_λ	W_λ
(1)	(2)	(3)	(4)	(5)	(6)	(7)	(8)	(9)	(10)	(11)	(12)	(13)	(14)	(15)	(16)	(17)	(18)	(19)	(20)	(21)
1231	1	0	12.6	9.2	<0.12	...	...	...	...	...	0.04	-0.97	0.34	-9.26	0.13	-3.65	...	...	...	...
	2	1	...	5.8	0.22	-1.83	0.28	-2.34	0.21	-1.76	0.35	-2.76	4.52	-35.14	1.47	-11.25	0.42	-3.31	0.48	-3.80
	3	0	10.3	11.5	<0.42	...	...	...	...	...	0.08	-0.89	1.21	-13.88	0.48	-5.45	0.12	-1.36	0.20	-2.33
1273	...	1	...	5.7	<0.31	...	...	...	...	...	0.06	-1.51	0.90	-21.61	0.34	-8.22	...	...	...	...
1291	...	1	...	5.0	0.63	-4.35	0.59	-4.02	0.95	-6.40	2.01	-11.44	3.17	-18.00	2.43	-13.82	0.44	-2.50	0.11	-0.63
1302	1	0	31.0	8.0	0.03	-5.17	...	...	0.05	-8.29	...	...	0.22	-51.11	0.04	-10.22	0.08	-18.74	0.06	-12.94
	2	0	17.2	6.9	<0.28	...	...	...	0.10	-3.69	0.03	-1.18	0.80	-36.10	0.26	-12.20	0.11	-4.88	0.09	-4.02
	3	1	...	5.8	0.24	-1.85	...	...	...	...	0.16	-1.22	3.09	-23.83	1.20	-9.31	0.33	-2.53	0.40	-3.04
	4	0	16.1	9.2	0.10	-2.43	0.06	-1.45	0.07	-1.78	0.15	-4.61	0.69	-21.94	0.28	-8.74	0.03	-1.01	0.07	-2.21
1326	1	0	19.5	6.9	0.03	-1.60	...	...	0.02	-1.14	...	-0.03	0.37	-20.57	0.07	-3.85	...	...	...	...
	2	0	13.8	2.3	0.05	-4.21	...	...	0.02	-2.23	0.01	-1.35	0.27	-28.06	0.07	-7.29	...	...	...	...
	3	1	...	6.9	0.26	-2.54	0.18	-1.78	0.06	-0.62	0.23	-2.72	1.94	-22.25	0.77	-9.09	0.38	-4.44	0.27	-3.12
	4	0	8.0	4.6	0.09	-0.95	0.08	-0.86	...	...	0.07	-0.89	1.15	-15.02	0.48	-6.37	0.19	-2.55	0.18	-2.47
1341	1	0	15.0	7.0	0.44	-10.64	...	...	...	...	0.10	-2.30	2.00	-47.08	0.51	-12.16	...	...	...	...
	2	0	5.0	4.0	0.37	-5.56	0.27	-4.07	...	...	0.36	-5.13	3.05	-44.70	1.19	-17.81	0.58	-9.02	0.60	-9.47
	3	1	...	5.0	1.55	-8.64	0.50	-2.87	0.51	-2.91	1.22	-8.34	9.44	-64.22	3.29	-22.49	1.67	-11.32	1.37	-9.33
	4	0	13.0	7.0	0.63	-3.20	0.48	-2.49	0.33	-1.73	0.74	-4.80	5.51	-35.62	2.38	-15.51	0.78	-5.10	0.60	-3.89
1346	1	1	...	9.2	3.42	-44.80	5.46	-75.63	16.38	-232.07	0.12	-2.68	12.43	-279.30	0.63	-14.40	0.91	-20.51	0.84	-18.99
	2	0	5.8	6.9	2.62	-33.30	4.35	-57.18	13.02	-173.08	0.10	-2.12	9.09	-193.96	0.38	-8.00	0.56	-12.35	0.67	-15.02
	3	0	16.1	12.6	1.23	-11.18	2.24	-20.36	5.73	-52.02	0.02	-0.25	5.35	-71.87	0.35	-4.63	0.49	-6.61	0.67	-8.89
	4	0	34.5	12.6	0.43	-3.80	1.04	-9.57	3.99	-37.01	...	...	3.20	-41.49	0.52	-6.80	0.35	-4.47	0.41	-5.35
1361	...	1	...	5.7	0.90	-8.13	1.76	-15.09	5.73	-50.37	2.59	-16.88	12.82	-82.95	8.64	-55.83	0.73	-4.42	1.05	-6.28
1363	1	0	14.9	4.6	<0.16	...	...	...	...	...	0.02	-0.51	0.45	-9.61	0.26	-5.74	0.07	-1.49	0.05	-1.11
	2	1	...	3.4	1.16	-36.52	...	...	...	...	0.02	-0.51	0.47	-12.32	0.15	-4.08	...	...	...	...
	3	0	19.5	4.6	0.09	-8.60	...	...	...	...	0.02	-0.51	0.27	-21.63	0.19	-15.51	...	...	...	...
1365	...	1	...	5.7	1.59	-2.86	1.92	-3.55	4.23	-7.87	1.79	-3.93	17.66	-38.78	8.67	-19.02	2.06	-4.52	2.21	-4.84
1379	1	0	11.5	8.0	1.34	-14.59	0.35	-4.04	0.86	-9.65	0.27	-3.82	5.60	-77.44	1.80	-24.88	0.77	-11.16	0.67	-9.88
	2	1	...	5.8	4.55	-9.45	0.75	-1.60	1.25	-2.68	0.94	-2.28	27.49	-65.19	8.25	-19.94	3.41	-8.59	3.16	-8.01
	3	1	...	4.6	2.57	-54.99	2.14	-48.60	6.41	-146.52	...	...	9.24	-276.82	0.83	-26.28	0.91	-28.44	0.59	-19.17
	4	0	6.9	5.8	1.37	-25.04	1.05	-20.62	2.91	-58.75	...	...	6.98	-170.01	0.48	-12.38	0.95	-24.07	0.56	-14.41
1433	1	0	5.0	5.0	0.20	-5.64	...	...	...	...	0.28	-8.26	1.13	-34.13	0.44	-13.14	0.26	-7.68	0.17	-5.02
	2	1	...	4.0	0.19	-2.00	...	...	...	...	0.59	-6.05	2.62	-27.02	1.17	-11.93	0.29	-3.02	0.18	-1.90
	3	0	6.0	4.0	<0.29	...	...	...	...	...	0.04	-1.28	0.84	-28.13	0.15	-5.33	0.11	-4.07	0.32	-12.21
1452	1	0	10.3	4.6	<0.07	...	...	...	...	...	0.04	-3.46	0.19	-18.27	0.08	-8.07	...	...	...	...
	2	1	...	6.9	0.22	-1.15	0.24	-1.22	0.13	-0.65	0.14	-0.78	2.34	-12.89	1.06	-5.87	...	...	...	...
	3	0	2.3	1.1	0.07	-0.85	0.08	-0.88	0.05	-0.61	0.10	-1.21	0.94	-11.45	0.44	-5.31	...	...	...	...
1466	...	1	...	5.7	3.42	-17.79	...	...	1.36	-7.13	4.64	-23.00	20.77	-102.53	12.79	-62.17	2.52	-12.41	3.20	-15.53
1485	1	0	37.9	5.8	0.23	-6.38	...	...	...	...	0.16	-5.52	1.41	-49.36	0.39	-13.58	0.18	-6.59	0.13	-4.85
	2	0	25.3	4.6	0.11	-2.68	...	...	0.04	-1.00	0.17	-4.96	0.81	-23.45	0.36	-10.51	0.10	-2.89	0.07	-2.05
	3	1	...	3.4	0.31	-1.05	0.44	-1.53	0.65	-2.32	1.77	-6.75	3.18	-12.20	3.90	-15.09	0.57	-2.27	0.53	-2.08
	4	0	29.9	8.0	<0.10	...	0.06	-1.23	...	...	0.06	-1.39	0.31	-7.29	0.15	-3.60	0.08	-1.79	0.04	-0.86

Table 5. Measured spectrophotometric data. Magnitudes and color indices of the spectral continuum.

(1) Markarian number
(2) Number of the emission-line region in the galaxy
(3) B magnitude ($\lambda_c = 4200$ Å, $\Delta\lambda = 300$Å)
(4) V magnitude ($\lambda_c = 5400$ Å, $\Delta\lambda = 300$Å)
(5) R magnitude ($\lambda_c = 6800$ Å, $\Delta\lambda = 200$Å)
(6) B-V color index
(7) V-R color index

Mrk (1)	H II (2)	m_B (3)	m_V (4)	m_R (5)	B-V (6)	V-R (7)
4	...	17.70	17.41	17.42	0.29	-0.01
10	1	15.78	15.40	15.09	0.38	0.31
	2	17.64	16.73	16.54	0.91	0.19
	3	21.00	22.72	19.96	-1.72	2.76
12	1	17.46	17.02	17.26	0.43	-0.23
	2	17.24	17.02	16.86	0.22	0.16
	3	17.12	16.92	16.80	0.21	0.12
	4	15.78	15.52	15.39	0.26	0.14
	5	17.21	17.10	16.97	0.11	0.12
	6	17.07	16.83	16.72	0.24	0.11
13	1	17.64	17.45	17.26	0.19	0.19
	2	17.44	17.21	17.02	0.23	0.19
21	1	18.94	18.74	18.35	0.20	0.38
	2	17.22	16.52	16.15	0.70	0.37
	3	16.42	15.72	15.38	0.70	0.34
	4	18.45	18.19	18.00	0.26	0.20
31	1	18.23	18.03	18.12	0.20	-0.09
	2	17.13	16.55	16.42	0.58	0.13
	3	19.13	18.47	18.13	0.65	0.34
38	...	17.05	16.64	16.37	0.41	0.27
39	1	17.16	16.98	16.94	0.18	0.04
	2	18.56	18.43	18.45	0.13	-0.02
42	1	17.91	17.11	17.13	0.80	-0.01
	2	16.86	16.26	15.82	0.60	0.44
52	...	14.72	14.49	14.45	0.23	0.04
58	...	17.11	16.55	16.57	0.56	-0.02
78	...	16.33	15.51	15.01	0.82	0.50
86	1	15.90	15.73	15.55	0.17	0.18
	2	15.33	15.17	15.10	0.15	0.08
87	...	16.41	15.63	15.18	0.78	0.45
90	1	17.84	16.18	15.76	1.66	0.41
	2	17.59	16.40	15.94	1.19	0.46
	3	19.01	16.98	16.54	2.03	0.44
114	...	16.00	15.38	14.96	0.62	0.41
122	1	18.86	17.69	17.18	1.17	0.51
	2	16.32	15.50	15.01	0.83	0.49
	3	18.39	17.60	17.18	0.79	0.42
133	1	...	17.03	16.71	...	0.32
	2	16.15	15.41	15.03	0.74	0.38
	3	18.65	16.32	15.94	2.33	0.38
	4	...	18.12	17.38	...	0.74
152	1	16.85	16.56	16.41	0.29	0.15
	2	17.25	16.75	16.52	0.50	0.24
161	1	18.48	17.07	16.85	1.41	0.22
	2	16.51	15.93	15.58	0.58	0.35
	3	17.85	16.85	16.61	1.00	0.24
179	1	18.02	17.61	17.40	0.41	0.22
	2	16.98	16.25	15.89	0.73	0.36
	3	18.10	17.84	17.52	0.27	0.32
185	1	17.38	16.80	16.66	0.58	0.14
	2	16.33	15.50	15.12	0.84	0.38
	3	17.64	17.23	16.81	0.41	0.41
	4	19.01	18.51	18.56	0.50	-0.05
188	1	16.87	16.47	16.22	0.40	0.25
	2	16.17	15.45	15.06	0.72	0.40
	3	16.91	16.44	16.14	0.46	0.30
213	1	16.23	16.05	15.80	0.18	0.25
	2	13.75	13.28	12.87	0.47	0.41
271	1	16.34	15.60	15.17	0.74	0.43
	2	17.07	16.64	16.18	0.42	0.46
	3	16.67	16.06	15.70	0.60	0.37
300	...	16.23	15.59	15.20	0.64	0.39
306	1	17.35	17.36	17.34	-0.01	0.02
	2	17.15	17.10	17.06	0.04	0.04
	3	17.36	17.27	17.25	0.10	0.02
	4	16.48	16.35	16.32	0.13	0.03
307	1	18.46	18.30	18.06	0.17	0.23
	2	17.45	17.22	17.04	0.23	0.18
	3	16.10	15.75	15.56	0.35	0.19
	4	18.48	18.26	18.01	0.22	0.25
	5	17.73	17.57	17.37	0.16	0.20
323	1	...	16.95	16.53	...	0.42
	2	19.00	17.37	17.00	1.63	0.36
	3	17.11	15.69	15.17	1.42	0.52
	4	...	16.98	16.37	...	0.62
332	1	17.19	16.91	16.68	0.27	0.24
	2	15.61	15.04	14.75	0.57	0.29
	3	16.57	16.12	15.79	0.45	0.33
	4	17.59	17.18	16.81	0.41	0.37
353	...	15.97	15.42	15.00	0.55	0.42
373	...	16.44	15.92	15.66	0.52	0.26
384	1	15.28	14.58	14.01	0.70	0.57
	2	16.00	15.35	15.09	0.64	0.27
401	1	19.87	17.00	16.65	2.87	0.35
	2	14.79	14.60	14.35	0.19	0.25
412	...	16.04	15.95	15.87	0.09	0.09
446	1	18.36	17.98	17.82	0.38	0.17
	2	15.41	14.96	14.68	0.46	0.28
	3	19.54	18.75	18.28	0.78	0.47
471	...	16.30	15.51	15.21	0.80	0.30
479	1	16.48	16.23	16.10	0.25	0.13
	2	17.23	17.06	16.89	0.17	0.17
489	1	17.10	16.88	16.85	0.22	0.03
	2	15.41	15.21	15.14	0.20	0.07
	3	17.73	17.38	17.17	0.35	0.20
534	1	14.33	14.01	13.77	0.32	0.24
	2	...	17.57	17.16	...	0.41
545	1	14.11	13.68	13.43	0.44	0.25
	2	17.36	17.08	16.84	0.28	0.24
571	...	17.17	15.65	15.32	1.52	0.34
575	1	18.08	17.39	17.07	0.69	0.33
	2	16.27	15.79	15.41	0.48	0.39
593	...	15.76	15.21	15.02	0.55	0.20
602	...	16.39	15.47	14.96	0.92	0.51
617	...	16.04	15.33	14.78	0.71	0.55
618	1	16.59	16.18	16.00	0.42	0.18
	2	17.57	17.26	17.11	0.31	0.15
620	...	15.43	14.54	14.01	0.88	0.54
665	1	16.84	15.95	15.49	0.89	0.46
	2	17.55	17.14	16.66	0.41	0.48
691	1	15.89	15.90	15.70	-0.01	0.20
	2	14.47	14.41	14.15	0.06	0.26
708	...	15.72	14.79	14.35	0.94	0.44
710	1	16.57	16.07	15.74	0.50	0.33
	2	16.26	16.21	15.99	0.05	0.23
	3	16.12	16.11	15.91	0.01	0.21
712	1	17.46	17.23	17.13	0.23	0.10
	2	17.70	17.42	17.24	0.29	0.18
	3	17.79	17.59	17.51	0.20	0.08

Mrk (1)	H II (2)	m_B (3)	m_V (4)	m_R (5)	B-V (6)	V-R (7)
718	1	18.63	17.78	17.26	0.85	0.52
	2	16.84	15.87	15.28	0.97	0.59
	3	18.60	18.09	17.82	0.52	0.27
731	1	16.82	15.90	15.42	0.92	0.48
	2	16.34	15.91	15.50	0.43	0.41
752	1	17.20	16.89	16.76	0.32	0.13
	2	17.45	17.19	17.12	0.26	0.07
759	...	16.75	15.68	15.23	1.07	0.45
781	1	17.02	16.58	16.48	0.44	0.10
	2	15.68	15.21	14.99	0.47	0.23
	3	17.43	17.03	16.91	0.40	0.12
	4	17.48	17.24	17.19	0.23	0.05
803	...	15.79	15.77	15.70	0.02	0.06
804	1	17.93	17.67	17.51	0.26	0.16
	2	17.22	16.89	16.68	0.34	0.21
	3	18.19	17.79	17.58	0.41	0.21
814	1	18.99	18.52	18.44	0.47	0.08
	2	17.73	17.15	16.92	0.59	0.23
	3	16.51	15.60	15.17	0.91	0.43
	4	17.81	17.10	16.76	0.71	0.34
	5	19.04	18.50	18.14	0.54	0.36
	6	20.98	20.81	20.44	0.17	0.37
860	1	18.01	17.65	17.42	0.35	0.24
	2	17.93	17.56	17.30	0.36	0.26
	3	17.73	17.26	17.00	0.47	0.26
	4	17.58	17.14	16.85	0.44	0.29
874	1	16.71	16.66	16.70	0.05	-0.03
	2	17.14	17.12	17.26	0.02	-0.14
	3	17.27	17.28	17.26	-0.01	0.02
1009	1	17.66	17.27	17.01	0.40	0.26
	2	16.01	15.12	14.73	0.90	0.38
	3	17.15	16.62	16.32	0.53	0.30
1026	1	...	18.44	18.02	...	0.41
	2	17.02	15.97	15.48	1.05	0.49
1050	...	16.17	15.38	14.99	0.79	0.40
1058	...	16.42	15.39	14.86	1.03	0.53
1066	...	15.51	14.62	13.93	0.89	0.69
1067	...	15.16	14.35	13.97	0.80	0.38
1073	1	16.74	16.22	15.96	0.51	0.27
	2	16.25	15.51	15.05	0.74	0.46
	3	17.82	17.09	16.76	0.73	0.33
1076	...	16.86	16.36	16.13	0.50	0.23
1086	1	20.44	18.06	17.42	2.38	0.64
	2	17.15	16.31	15.91	0.84	0.39
	3	17.94	17.30	16.94	0.64	0.36
1088	...	14.74	13.96	13.53	0.78	0.43

Mrk (1)	H II (2)	m_B (3)	m_V (4)	m_R (5)	B-V (6)	V-R (7)
1171	1	17.17	16.32	15.95	0.85	0.36
	2	15.75	15.17	14.86	0.58	0.31
	3	17.90	17.49	17.25	0.42	0.24
1180	...	15.56	14.35	13.76	1.21	0.60
1194	...	15.10	14.45	14.10	0.64	0.35
1200	...	16.25	15.43	14.98	0.82	0.46
1231	1	18.02	17.49	14.09	0.53	3.40
	2	15.18	14.37	13.97	0.80	0.40
	3	16.98	16.41	16.14	0.57	0.27
1273	...	18.25	17.36	16.95	0.88	0.41
1302	1	19.94	19.78	19.40	0.16	0.38
	2	18.42	17.88	17.70	0.54	0.18
	3	16.96	16.11	15.71	0.85	0.41
	4	18.02	17.50	17.29	0.52	0.21
1326	1	18.68	18.07	17.84	0.61	0.23
	2	19.32	18.80	18.53	0.52	0.27
	3	16.92	16.44	16.14	0.48	0.30
	4	17.02	16.54	16.29	0.48	0.25
1341	1	...	17.37	16.94	...	0.43
	2	18.41	16.91	16.48	1.50	0.43
	3	16.28	15.92	15.57	0.36	0.35
	4	16.29	15.79	15.51	0.50	0.28
1346	1	16.92	16.92	16.88	0.00	0.03
	2	16.85	16.86	16.88	-0.01	-0.02
	3	16.55	16.39	16.32	0.17	0.07
	4	16.68	16.41	16.27	0.27	0.14
1361	...	17.13	16.11	15.45	1.03	0.66
1363	1	17.91	17.19	16.87	0.72	0.32
	2	18.57	17.58	17.13	0.99	0.45
	3	19.86	18.87	18.35	0.99	0.52
1365	...	15.11	14.61	14.51	0.50	0.10
1379	1	16.93	16.60	16.42	0.33	0.18
	2	15.30	14.79	14.51	0.52	0.28
	3	17.48	17.48	17.31	0.00	0.18
	4	17.48	17.26	17.05	0.21	0.22
1433	1	18.18	17.56	17.17	0.62	0.39
	2	17.13	16.49	16.03	0.64	0.46
	3	18.18	17.74	17.40	0.43	0.34
1452	1	19.00	18.61	18.42	0.39	0.20
	2	16.32	15.67	15.33	0.65	0.34
	3	17.23	16.50	16.21	0.73	0.29
1466	...	16.38	15.69	15.19	0.69	0.51
1485	1	18.14	17.58	17.41	0.56	0.17
	2	17.57	17.35	17.19	0.22	0.16
	3	15.95	15.30	14.98	0.66	0.31
	4	17.78	17.18	16.90	0.60	0.28

Table 6. Derived spectrophotometric parameters

(1) Markarian number

(2) Number of the emission-line region in the galaxy

(3) Position: nuclear (= 1) or extranuclear (= 0) emission-line region

(4) Distance of the galaxy (in Mpc with $H_0 = 75$ kms^{-1}Mpc^{-1})

(5) Distance between extranuclear emission-line regions and the galaxy nucleus (in kpc)

(6) Size of emission-line regions (in kpc)

(7) Reddening coefficient $c_{H\beta}$ (in magnitudes)

(8) Electronic density (in cm^{-3})

(9) log([N II]λ6583/H$\alpha\lambda$6563)

(10) log([S II]$\lambda\lambda$6716,6731/H$\alpha\lambda$6563)

(11) log([O III]λ5007/H$\beta\lambda$4861)

(12) Results of the spectral classification (see text for details): SBNG = Starburst Nucleus Galaxy; H IIG = H II Galaxy; H II = extranuclear H II region; LIN = LINER; Sey 1 = Seyfert 1; Sey 2 = Seyfert 2; SBNG,LIN ? = ambiguous classification between starburst and LINER; H II ? = uncertain classification; ? = unknown spectral type

(13) Absolute Hα flux corrected for reddening ($\times$ 10^{-14} erg cm^{-2}s^{-1})

(14) Absolute Hα luminosity (erg s^{-1}). A lower limit (:) on both the Hα flux and luminosity is given if the reddening coefficient $c_{H\beta}$ has not been estimated

Mrk	H II		D	H II		$c_{H\beta}$	n_e	[N II]/Hα	[S II]/Hα	[O III]/Hβ	S.Type	I(Hα)	log(L$_{H\alpha}$)	
	num	pos	[Mpc]	dist	size	[mag]	[cm^{-3}]						[erg s^{-1}]	
(1)	(2)	(3)	(4)	(5)	(6)	(7)	(8)	(9)	(10)	(11)	(12)	(13)	(14)	
4	...	1	71.8	...	2.4	...	2041	-1.15	-0.62	...	SBNG	3.22	40.30	:
10	1	1	117.7	...	1.3	...	...	...	...	...	Sey 1	...	...	
	2	0	...	8.5	4.6	...	...	-0.56	...	...	HII ?	1.26	40.32	:
	3	0	...	24.9	2.0	...	...	-1.03	...	...	HII ?	0.55	39.96	:
12	1	0	54.4	5.8	2.1	0.363	231	-0.67	-0.51	0.36	HII	2.56	39.96	
	2	0	...	3.3	1.5	0.014	257	-0.67	-0.62	-0.03	HII	2.49	39.95	
	3	0	...	1.8	0.9	0.448	...	-0.54	-0.56	...	HII	4.10	40.16	
	4	1	...	...	2.1	0.558	...	-0.59	-0.60	-0.70	SBNG	28.23	41.00	
	5	0	...	2.1	1.2	0.241	...	-0.42	-0.47	...	HII	3.02	40.03	
	6	0	...	3.9	1.8	0.541	...	-0.70	...	0.08	HII	4.11	40.16	
13	1	1	20.0	...	0.3	0.172	257	-0.89	-0.81	0.21	SBNG	7.24	39.54	
	2	0	...	0.4	0.3	0.647	...	-0.99	-0.76	0.11	HII	20.01	39.98	
21	1	0	113.7	8.9	3.8	...	...	-0.52	...	...	HII ?	0.25	39.59	:
	2	1	...	...	1.3	1.230	...	-0.55	...	-0.66	SBNG	15.93	41.39	
	3	0	...	1.9	1.3	...	...	-0.35	...	...	HII ?	2.33	40.56	:
	4	0	...	10.1	5.1	...	...	-0.15	...	...	HII ?	0.47	39.86	:
31	1	0	104.9	9.9	4.7	...	...	-0.47	...	...	HII ?	0.62	39.91	:
	2	1	...	...	1.8	0.616	101	-0.56	-0.58	-0.57	SBNG	9.89	41.12	
	3	0	...	5.3	1.8	...	...	-0.62	...	...	HII ?	0.47	39.79	:
38	...	1	144.5	...	4.8	1.125	480	-0.50	-0.55	0.07	SBNG	14.50	41.56	
39	1	1	146.1	...	4.8	0.444	...	-0.85	-0.52	0.11	SBNG	3.19	40.90	
	2	0	...	5.6	4.0	0.684	...	-0.74	-0.48	0.09	HII	1.26	40.50	
42	1	0	96.6	4.3	1.1	0.911	...	-0.60	-0.73	-0.24	HII	2.26	40.40	
	2	1	...	...	1.1	0.033	...	-0.41	-1.52	-0.23	Sey 1	11.56	41.11	
52	...	1	27.3	...	0.6	0.005	563	-0.33	-0.75	-0.20	SBNG	78.03	40.84	
58	...	1	73.8	...	2.5	...	1081	-0.44	-0.48	...	SBNG	1.55	40.01	:
78	...	1	151.6	...	4.2	0.710	172	-0.07	-0.33	1.04	Sey 2	66.57	42.26	
79	...	1	89.1	...	4.2	...	...	...	...	...	Sey 1	...	...	
86	1	0	6.2	1.0	0.3	0.307	...	-0.98	...	0.57	HII	5.37	38.39	
	2	1	...	...	0.2	0.109	64	-0.85	-0.67	0.28	HIIG	44.75	39.31	
87	...	1	48.3	...	1.6	...	257	-0.40	-0.56	...	SBNG	4.98	40.14	:
90	1	0	57.2	1.9	3.0	0.779	1040	-0.45	-0.86	...	HII	11.14	40.64	
	2	1	...	...	1.1	1.225	737	-0.10	-0.69	...	SBNG,LIN ?	20.67	40.91	
	3	0	...	2.8	2.2	...	...	-0.37	...	...	HII ?	1.08	39.63	:
114	...	1	101.2	...	2.9	...	795	-0.30	-1.16	...	SBNG	7.08	40.94	:
122	1	0	89.0	3.9	1.7	0.177	...	-0.38	...	...	HII ?	1.87	40.25	
	2	1	...	...	1.3	...	...	-0.28	...	...	SBNG ?	5.63	40.73	:
	3	0	...	4.3	1.7	...	...	-0.61	...	...	HII ?	1.42	40.13	:
133	1	0	29.3	1.1	0.7	...	...	-0.48	...	...	HII ?	0.98	39.00	:
	2	1	...	...	0.6	0.664	682	-0.40	-0.71	-0.83	SBNG	40.20	40.61	
	3	0	...	1.3	1.1	0.378	31	-0.53	-0.57	...	HII	4.59	39.68	
	4	0	...	2.8	0.7	...	...	-0.34	...	...	HII ?	0.59	38.78	:
141	...	1	164.4	...	1.0	...	...	...	...	...	Sey 1	...	...	
152	1	1	92.7	...	1.0	0.404	...	-0.33	...	...	SBNG ?	4.83	40.70	
	2	0	...	3.6	2.6	...	...	0.02	...	...	LIN ?	0.93	39.98	:
161	1	0	80.2	4.7	1.6	0.830	...	-0.45	-0.68	-0.04	HII	15.07	41.07	
	2	1	...	...	0.8	1.150	...	-0.26	-0.78	-0.08	SBNG	37.90	41.47	
	3	0	...	4.3	1.6	0.646	...	-0.44	-0.73	-0.22	HII	16.25	41.10	
179	1	1	45.6	...	1.5	0.011	...	-0.60	-0.55	...	SBNG	0.93	39.37	
	2	0	...	3.3	0.8	...	...	-0.10	...	...	LIN ?	0.60	39.18	:
	3	0	...	7.6	1.3	...	...	-0.08	...	...	LIN ?	0.86	39.33	:
185	1	0	42.0	3.3	2.1	0.469	...	-0.66	...	...	HII ?	2.06	39.64	
	2	1	...	...	1.2	...	219	-0.38	-0.69	...	SBNG	3.47	39.87	:
	3	0	...	4.7	2.3	0.661	...	-0.53	-0.62	...	HII	3.69	39.89	
	4	0	...	6.8	1.2	0.997	926	-0.74	-0.70	...	HII	4.99	40.01	
188	1	0	33.1	2.8	1.3	0.880	...	-0.68	...	-0.95	HII	21.61	40.45	
	2	1	...	...	0.7	0.982	...	-0.66	-0.86	-0.87	SBNG	22.50	40.47	
	3	0	...	1.8	0.7	1.127	1169	-0.61	-0.80	-1.08	HII	25.24	40.51	
213	1	0	40.2	3.6	1.0	0.509	563	-0.63	-0.77	-0.03	HII	28.16	40.74	
	2	1	...	...	1.0	0.728	284	-0.33	-0.74	0.26	SBNG	340.05	41.81	
271	1	1	102.0	...	5.7	0.814	...	-0.22	...	0.05	SBNG,LIN ?	11.24	41.15	
	2	0	...	6.8	4.0	...	...	-0.26	...	...	HII	1.21	40.18	:
	3	1	...	...	4.0	0.852	...	-0.14	...	0.84	Sey 2	6.42	40.90	
291	...	1	141.7	...	3.5	...	...	...	...	...	Sey 1	...	...	

Mrk	H II num	pos	D [Mpc]	H II dist	size	$c_{H\beta}$ [mag]	n_e [cm^{-3}]	[N II]/Hα	[S II]/Hα	[O III]/Hβ	S.Type	I(Hα)	log($L_{H\alpha}$) [erg s^{-1}]	
(1)	(2)	(3)	(4)	(5)	(6)	(7)	(8)	(9)	(10)	(11)	(12)	(13)	(14)	
300	...	1	157.1	...	3.5	1.421	709	-0.27	-0.62	-0.37	SBNG	46.71	42.14	
306	1	0	77.3	3.4	1.9	0.253	608	-0.72	-0.54	0.17	HII	3.45	40.39	
	2	1	...	...	1.5	0.296	858	-0.48	-0.49	-0.12	SBNG	4.69	40.53	
	3	0	...	1.9	1.0	0.526	195	-0.57	-0.59	-0.03	HII	6.38	40.66	
	4	0	...	2.9	3.4	0.395	130	-0.60	-0.59	-0.03	HII	10.85	40.89	
307	1	0	76.7	4.3	1.0	0.114	137	-0.47	-0.42	0.14	HII	0.67	39.67	
	2	0	...	2.4	1.4	0.748	...	-0.41	-0.45	-0.22	HII	6.54	40.66	
	3	1	...	...	1.4	0.628	709	-0.46	-0.63	-0.63	SBNG	11.92	40.91	
	4	0	...	1.9	1.4	0.612	425	-0.41	-0.52	...	HII	1.57	40.04	
	5	0	...	3.9	1.4	0.401	...	-0.53	-0.53	-0.09	HII	3.41	40.38	
323	1	0	59.3	3.7	2.9	0.390	298	-0.47	-0.62	...	HII	4.89	40.31	
	2	0	...	0.9	0.6	0.824	...	-0.62	-1.18	...	HII	9.70	40.61	
	3	1	...	...	2.6	0.763	...	-0.54	-0.99	...	SBNG	29.86	41.10	
	4	0	...	4.0	2.0	0.607	...	-0.50	...	...	HII ?	4.59	40.29	
332	1	0	34.2	1.7	1.1	0.649	...	-0.61	-0.70	-0.66	HII	10.41	40.17	
	2	1	...	...	0.4	0.814	358	-0.15	-0.40	-0.81	SBNG,LIN ?	25.76	40.56	
	3	0	...	1.5	1.3	0.876	...	-0.58	-0.70	-0.67	HII	18.77	40.41	
	4	0	...	3.9	1.1	0.307	...	-0.21	...	-0.10	HII	2.48	39.54	
353	...	1	64.0	...	2.0	1.226	270	-0.18	-0.59	0.01	SBNG,LIN ?	79.18	41.59	
373	...	1	79.4	...	1.8	0.980	585	-0.33	-0.60	-0.11	SBNG	50.00	41.58	
374	...	1	171.2	...	1.8	...	...	...	...	...	Sey 1	...	...	
382	...	1	134.5	...	2.0	...	...	...	...	...	Sey 1	...	...	
384	1	0	61.7	3.1	1.4	0.804	...	-0.33	-0.56	...	HII	2.49	40.06	
	2	1	...	...	1.0	1.008	1169	-0.31	-0.77	...	SBNG	34.33	41.20	
401	1	0	22.0	1.1	0.7	0.169	2774	-0.38	-0.59	...	HII	2.25	39.11	
	2	1	...	...	0.4	0.628	1000	-0.30	-0.68	-0.67	SBNG	60.79	40.55	
412	...	1	59.2	...	1.6	0.334	82	-1.08	-0.78	0.49	HIIG	29.43	41.09	
446	1	0	94.9	7.9	2.1	0.541	...	-0.54	...	...	HII ?	3.10	40.51	
	2	1	...	...	2.1	1.159	...	-0.40	...	-0.78	SBNG	47.63	41.71	
	3	0	...	9.5	2.6	...	...	-0.59	...	...	HII ?	0.84	39.96	:
471	...	1	137.8	...	3.8	...	270	0.07	-0.35	...	Sey 2	2.23	40.71	:
474	...	1	146.1	...	1.8	...	...	...	...	...	Sey 1	...	...	
479	1	1	81.6	...	1.8	0.686	...	-0.76	-0.76	...	SBNG	23.56	41.28	
	2	0	...	7.3	1.8	0.358	407	-0.77	-0.66	0.15	HII	7.96	40.80	
489	1	0	129.3	5.8	4.3	...	1040	-0.48	-0.57	...	HII	1.42	40.45	:
	2	1	...	...	3.6	0.863	...	-0.60	-0.63	-0.09	SBNG	48.74	41.99	
	3	0	...	5.0	2.2	...	374	-0.71	-0.71	-0.46	HII	1.31	40.42	:
493	...	1	127.6	...	1.8	...	...	...	...	...	Sey 1	...	...	
534	1	1	70.3	...	2.0	1.036	130	-0.40	-0.77	0.04	SBNG	228.22	42.13	
	2	0	...	3.1	1.0	0.913	...	-0.59	-0.66	0.10	HII	15.44	40.96	
545	1	1	63.1	...	2.0	0.684	...	-0.16	-0.47	-0.40	SBNG	93.16	41.65	
	2	0	...	6.0	1.2	0.541	73	-0.31	-0.66	-0.39	HII	9.84	40.67	
571	...	1	69.5	...	1.3	1.076	...	-0.36	-0.78	...	SBNG	37.20	41.33	
575	1	0	74.2	4.3	1.8	0.338	...	-0.55	-0.69	...	HII	3.91	40.41	
	2	1	...	...	0.7	0.865	327	-0.32	-0.77	...	SBNG	28.37	41.27	
593	...	1	110.9	...	3.1	...	...	-0.25	...	...	SBNG,LIN ?	2.37	40.54	:
602	...	1	38.1	...	0.7	1.330	298	-0.41	-0.63	-0.52	SBNG	136.80	41.38	
617	...	1	62.4	...	1.4	1.557	826	-0.15	-0.65	-0.10	SBNG,LIN ?	324.41	42.18	
618	1	1	141.3	...	2.4	...	...	...	...	-0.19	Sey 1	...	...	
	2	0	...	7.9	3.9	...	...	-0.49	-0.75	...	HII	1.41	40.53	:
620	...	1	25.7	...	0.5	1.210	1374	-0.12	-0.42	0.79	Sey 2	157.17	41.09	
665	1	1	102.5	...	1.1	1.091	1374	-0.35	-0.76	0.08	SBNG	17.56	41.35	
	2	0	...	4.6	2.9	0.772	91	-0.65	-0.82	-0.44	HII	3.93	40.70	
691	1	0	45.7	2.6	1.7	0.539	219	-1.06	-0.68	0.20	HII	56.20	41.14	
	2	1	...	...	1.4	0.766	826	-0.67	-0.77	-0.63	SBNG	230.06	41.75	
708	...	1	25.3	...	0.7	1.061	161	-0.36	-0.53	-0.69	SBNG	135.83	41.01	
710	1	0	18.3	1.0	0.9	0.697	64	-0.59	-0.62	-0.61	HII	30.95	40.09	
	2	0	...	0.3	0.3	0.341	327	-0.48	-0.70	-0.51	HII	26.09	40.01	
	3	1	...	...	0.4	0.340	184	-0.43	-0.68	-0.50	SBNG	38.37	40.19	
712	1	0	59.5	1.7	1.3	0.250	82	-0.89	-1.02	0.46	HII	14.02	40.78	
	2	1	...	...	0.7	0.272	...	-0.64	-0.65	0.31	SBNG	2.72	40.06	
	3	0	...	2.3	2.3	...	161	-0.43	-0.38	0.04	HII,LIN ?	0.89	39.58	:
718	1	0	111.5	4.4	1.2	1.584	374	-0.60	-0.84	...	HII	10.84	41.21	
	2	1	...	...	1.9	1.210	130	-0.42	-1.06	-0.76	SBNG	19.45	41.46	
	3	0	...	6.2	1.2	1.014	...	-0.48	-0.90	-0.72	HII	4.26	40.80	

Mrk	H II		D	H II		$c_{H\beta}$	n_e	[N II]/Hα	[S II]/Hα	[O III]/Hβ	S.Type	I(Hα)	log(L$_{H\alpha}$)	
	num	pos	[Mpc]	dist	size	[mag]	[cm^{-3}]						[erg s^{-1}]	
(1)	(2)	(3)	(4)	(5)	(6)	(7)	(8)	(9)	(10)	(11)	(12)	(13)	(14)	
731	1	0	17.8	0.3	0.3	...	657	-0.35	-0.46	...	HII	4.68	39.25	:
	2	1	...	...	0.3	1.278	520	-0.35	-0.64	-0.87	SBNG	118.67	40.65	
752	1	1	80.2	...	3.6	0.560	...	-0.62	-0.82	-0.10	SBNG	6.12	40.67	
	2	0	...	4.0	3.1	0.503	...	-0.69	-0.81	0.15	HII	3.68	40.45	
759	...	1	28.1	...	0.7	0.887	858	-0.34	-0.86	...	SBNG	22.67	40.33	
766	...	1	51.1	...	1.8	...	...	...	...	...	Sey 1	...	...	
781	1	0	37.1	4.5	2.5	0.524	...	-0.54	-0.84	-0.15	HII	5.27	39.94	
	2	1	...	...	1.0	0.629	91	-0.47	-0.72	-1.01	SBNG	33.91	40.75	
	3	0	...	4.1	1.0	...	...	-0.64	-0.59	...	HII	1.75	39.46	:
	4	0	...	5.8	1.7	0.680	...	-0.63	-0.56	0.12	HII	4.13	39.83	
803	...	1	54.7	...	1.5	0.115	...	-1.07	-0.81	0.55	HIIG	16.26	40.77	
804	1	0	71.6	2.4	3.2	0.742	...	-0.61	-0.66	-0.16	HII	5.53	40.53	
	2	1	...	...	2.4	0.781	82	-0.40	-0.61	-0.19	SBNG	6.47	40.60	
	3	0	...	2.4	4.0	0.971	257	-0.39	-0.55	0.00	HII	10.40	40.81	
814	1	0	53.0	5.9	1.5	1.196	442	-0.51	-0.41	0.00	HII,LIN ?	3.21	40.03	
	2	0	...	3.0	1.8	1.098	207	-0.49	-0.56	-0.01	HII	6.29	40.33	
	3	1	...	...	1.2	1.072	195	-0.29	-0.52	-0.76	SBNG	24.87	40.91	
	4	0	...	2.7	1.5	...	425	-0.23	-0.38	...	HII,LIN ?	0.51	39.24	:
	5	0	...	6.2	1.5	...	...	-0.48	...	...	HII ?	0.30	39.01	:
	6	0	...	11.2	0.6	...	...	-1.04	...	...	HII ?	0.11	38.57	:
860	1	1	92.8	...	2.6	0.432	...	-0.58	-0.73	0.52	HIIG	4.24	40.64	
	2	0	...	2.1	2.6	0.279	500	-0.49	-0.64	0.48	HII	3.71	40.58	
	3	0	...	2.1	2.1	0.625	...	-0.40	-0.98	-0.53	HII	6.99	40.86	
	4	1	...	...	2.1	0.629	...	-0.22	-0.81	-0.31	SBNG	7.80	40.91	
874	1	1	56.7	...	1.6	0.374	...	-0.93	-0.45	0.33	LIN,SBNG ?	5.86	40.35	
	2	0	...	1.3	0.9	0.135	56	-1.03	-0.70	0.39	HII	5.60	40.33	
	3	1	...	...	0.9	0.265	82	-0.90	-0.62	0.31	SBNG	8.39	40.51	
1009	1	0	57.0	5.7	1.9	0.690	...	-0.52	-0.56	0.05	HII	5.69	40.35	
	2	1	...	...	1.3	0.803	140	-0.48	-0.61	-0.61	SBNG	26.92	41.01	
	3	0	...	4.8	2.2	0.898	...	-0.42	-0.54	-0.47	HII	7.37	40.46	
1026	1	0	52.7	5.6	1.8	...	...	-0.96	-0.60	...	HII	1.24	39.62	:
	2	1	...	...	1.3	1.367	...	-0.43	-0.61	-0.32	SBNG	41.35	41.14	
1050	...	1	67.0	...	1.6	1.239	1494	-0.29	-0.70	...	SBNG	88.09	41.68	
1058	...	1	69.5	...	2.3	1.346	1627	-0.24	-0.41	0.98	Sey 2	55.54	41.51	
1066	...	1	49.5	...	1.3	1.103	826	-0.06	-0.40	0.52	Sey 2	314.61	41.97	
1067	...	1	57.1	...	1.6	...	244	-0.22	-0.66	...	SBNG	6.78	40.42	:
1073	1	0	94.8	4.8	4.2	0.836	...	-0.55	-0.96	0.07	HII	28.60	41.49	
	2	1	...	...	2.1	0.489	244	-0.04	-0.51	0.77	Sey 2	49.80	41.73	
	3	0	...	5.3	1.6	...	...	-0.25	...	...	HII ?	3.27	40.55	:
1076	...	1	96.3	...	3.2	0.945	1000	-0.57	-0.92	-0.52	SBNG	25.44	41.45	
1086	1	0	119.3	4.0	2.9	...	...	-0.32	...	...	HII ?	0.66	40.05	:
	2	1	...	...	2.3	1.126	130	-0.29	-0.60	...	SBNG	27.12	41.67	
	3	0	...	2.9	2.3	...	608	-0.42	0.06	...	HII,LIN ?	1.15	40.29	:
1088	...	1	60.4	...	1.7	1.046	461	-0.25	-0.62	-0.95	SBNG	150.46	41.81	
1171	1	0	70.8	8.3	2.4	0.148	3111	-0.45	-0.61	-0.78	HII	2.17	40.11	
	2	1	...	...	2.4	1.175	585	-0.48	-0.89	...	SBNG	50.47	41.48	
	3	0	...	7.1	1.6	1.021	184	-0.50	-0.83	...	HII	4.91	40.47	
1180	...	1	61.2	...	1.7	...	...	0.02	-0.68	...	SBNG,LIN ?	3.71	40.22	:
1194	...	1	58.7	...	2.6	1.356	...	-0.39	-0.93	...	SBNG	153.16	41.80	
1200	...	1	102.9	...	2.8	...	...	-0.14	...	...	SBNG,LIN ?	3.51	40.65	:
1231	1	0	149.0	9.1	6.6	...	...	-0.42	...	...	HII ?	0.41	40.04	:
	2	1	...	...	4.2	1.676	1081	-0.52	-0.76	-0.40	SBNG	62.54	42.21	
	3	0	...	7.5	8.3	...	4320	-0.40	-0.58	...	HII	1.38	40.57	:
1273	...	1	107.0	...	2.9	...	...	-0.42	...	...	SBNG ?	0.98	40.13	:
1291	...	1	47.0	...	1.8	0.739	...	-0.11	-0.76	0.39	SBNG,LIN ?	9.84	40.42	
1302	1	0	73.1	11.0	2.9	1.230	137	-0.74	-0.20	0.35	HII,LIN ?	1.45	39.97	
	2	0	...	6.1	2.4	...	270	-0.49	-0.60	...	HII	0.84	39.73	:
	3	1	...	...	2.0	1.108	1319	-0.45	-0.69	...	SBNG	18.35	41.07	
	4	0	...	5.7	3.3	0.478	...	-0.43	-0.89	-0.43	HII	1.57	40.00	
1326	1	0	17.6	1.7	0.6	0.967	...	-0.77	...	-0.56	HII	1.79	38.81	
	2	0	...	1.2	0.2	0.411	...	-0.62	...	-0.58	HII	0.54	38.30	
	3	1	...	...	0.6	0.604	64	-0.44	-0.53	-0.91	SBNG	5.34	39.30	
	4	0	...	0.7	0.4	0.636	541	-0.44	-0.56	...	HII	3.46	39.11	
1330	...	1	31.9	...	1.8	...	...	...	...	...	Sey 1	...	...	

Mrk	H II		D	H II		$c_{H\beta}$	n_e	[N II]/Hα	[S II]/Hα	[O III]/Hβ	S.Type	I(Hα)	log($L_{H\alpha}$)	
	num	pos	[Mpc]	dist	size	[mag]	[cm^{-3}]						[erg s^{-1}]	
(1)	(2)	(3)	(4)	(5)	(6)	(7)	(8)	(9)	(10)	(11)	(12)	(13)	(14)	
1341	1	0	14.6	1.1	0.5	0.433	...	-0.61	...	...	HII ?	4.05	39.01	
	2	0	...	0.4	0.3	1.034	765	-0.43	-0.46	...	HII	15.58	39.60	
	3	1	...	...	0.4	0.752	270	-0.47	-0.52	-0.60	SBNG	30.87	39.90	
	4	0	...	0.9	0.5	0.893	161	-0.39	-0.65	-0.53	HII	22.92	39.77	
1346	1	1	13.4	...	0.6	0.264	480	-1.30	-0.86	0.65	HIIG	18.77	39.61	
	2	0	...	0.4	0.4	0.189	1267	-1.38	-0.88	0.66	HII	12.27	39.41	
	3	0	...	1.0	0.8	0.367	2041	-1.20	-0.68	0.58	HII	9.66	39.32	
	4	0	...	2.2	0.8	0.755	1169	-0.81	-0.66	0.76	HII	10.68	39.36	
1361	...	1	90.4	...	2.5	1.833	2365	-0.19	-0.91	0.64	Sey 2	218.73	42.33	
1363	1	0	35.6	2.6	0.8	...	73	-0.24	-0.57	...	HII,LIN ?	0.54	38.92	:
	2	1	...	...	0.6	...	...	-0.56	...	...	SBNG ?	0.55	38.92	:
	3	0	...	3.4	0.8	...	...	-0.19	...	...	HII,LIN ?	0.29	38.65	:
1365	...	1	73.9	...	2.0	1.140	858	-0.33	-0.66	0.15	SBNG	106.86	41.85	
1379	1	0	34.4	1.9	1.3	0.359	374	-0.51	-0.61	-0.26	HII	9.97	40.15	
	2	1	...	...	1.0	0.762	500	-0.54	-0.65	-0.67	SBNG	91.26	41.11	
	3	1	...	...	0.8	0.260	...	-1.05	-0.80	0.37	SBNG	13.88	40.30	
	4	0	...	1.2	1.0	0.666	...	-1.17	-0.69	0.27	HII	19.63	40.45	
1433	1	0	254.5	6.2	6.2	0.565	...	-0.44	-0.46	...	HII	2.85	41.35	
	2	1	...	...	4.9	1.237	...	-0.39	-0.81	...	SBNG	18.79	42.16	
	3	0	...	7.4	4.9	...	...	-0.75	-0.29	...	HII,LIN ?	0.90	40.84	:
1452	1	0	90.0	4.5	2.0	...	...	-0.37	...	...	HII ?	0.21	39.31	:
	2	1	...	...	3.0	0.585	...	-0.41	...	-0.69	SBNG	6.64	40.81	
	3	0	...	1.0	0.5	0.647	...	-0.40	...	-0.70	HII	2.98	40.46	
1466	...	1	16.4	...	0.4	0.866	1558	-0.22	-0.59	-0.48	SBNG	79.97	40.41	
1485	1	0	31.8	5.8	0.9	0.689	82	-0.58	-0.69	...	HII	4.22	39.71	
	2	0	...	3.9	0.7	0.611	47	-0.39	-0.73	-0.70	HII	2.25	39.44	
	3	1	...	...	0.5	0.472	500	0.02	-0.54	-0.16	LIN,SBNG ?	7.63	39.97	
	4	0	...	4.6	1.2	...	...	-0.17	-0.41	...	HII ?	0.39	38.67	: